THESIS FOR THE DEGREE OF LICENTIATE OF ENGINEERING IN PHYSICS

Electrooxidation of glycerol and methanol on gold

MIKAEL VALTER

CHALMERS

Department of Physics
Division of Chemical Physics
CHALMERS UNIVERSITY OF TECHNOLOGY
Göteborg, Sweden 2018

Electrooxidation of glycerol and methanol on gold
MIKAEL VALTER

Department of Physics
Division of Chemical Physics
Chalmers University of Technology
SE-412 96 Göteborg
Sweden
Telephone: +46 (0)31-772 1000

Cover:
Products from glycerol electrooxidation. Image by Adam Arvidsson.

Chalmers Reproservice
Göteborg, Sweden 2018

Electrooxidation of glycerol and methanol on gold
Thesis for the degree of Licentiate of Engineering in Physics
MIKAEL VALTER
Department of Physics
Division of Chemical Physics
Chalmers University of Technology

Abstract

Burning of fossil fuels leads to excess CO_2 in the atmosphere, causing global warming, threatening civilisation and ecosystems worldwide. As a step in making the society fossil-independent, we need to replace oil, coal, and gas in the transportation sector with fuels originating from sustainable energy. Biodiesel is one such option, from which we get glycerol as a byproduct. With the help of electrooxidation, we can use glycerol as a feedstock to extract hydrogen gas, which may be for upgrading biofuels or used in proton exchange membrane (PEM) fuel cells. Methanol is another possible fuel in so called direct methanol fuel cells (DMFC), which raises the interest for studying methanol electrooxidation.

In this work, we study glycerol and methanol electrooxidation on gold. We use density functional theory, and verification by cyclic voltammetry, to study thermodynamics of reaction conditions and mechanisms for the electrooxidation mechanisms. Long range dispersion (van der Waals), which have been neglected in computations until recently, is investigated by assessing density van der Waals functionals. Furthermore, microsolvent effects are investigated by inclusion of explicit water molecules.

Keywords: DFT, electrochemistry, glycerol, methanol, gold, van der Waals

List of Publications

This thesis is based on the following appended papers:

Paper I:

Geometry and Electronic Propertiesof Glycerol Adsorbed on Bare and Transition-Metal Surface-Alloyed Au(111): A Density Functional Theory Study
Jonas Baltrusaitis, Mikael Valter, and Anders Hellman
J. Chem. Phys. C **120**.3 (2016), 1749–1757

Paper II:

Electrooxidation of Glycerol on Gold in Acidic Medium: A Combined Experimental and DFT Study
Mikael Valter, Michael Busch, Björn Wickman, Henrik Grönbeck, Jonas Baltrusaitis, and Anders Hellman
J. Phys. Chem. C, **122**.19 (2018), 10489-10494

Paper III:

van der Waals and Solvent Effects of Methanol Electrooxidation on Gold: a DFT Study
Mikael Valter and Anders Hellman
In manuscript

My contributions to the publications

Paper I
I performed the benchmarking calculations on gold properties (Table 1) and co-authored the the manuscript.

Paper II
I performed all the calculations and experiments and wrote the first draft of the paper.

Paper III
I performed all calculations and wrote the first draft of the manuscript.

Contents

Chapter 1

Introduction

While what we now call catalysis has been used throughout history, e.g. in fermentation of sugar to alcohol, there has not been any recorded attempts to characterise and explain the phenomenon until around 1800.[1] In 1798, the Scottish chemist Elizabeth Fulhame describes how water facilitates oxidation and reduction reactions. She explains that the reactions are dependent on the presence of water, that water is directly involved in the chemical process and that the amount of water remains the same at the start and the end of the reaction.[2] This property of the water, that it enables or facilitates a reaction without being consumed itself, makes it a *catalyst*. This term is derived from *catalysis* (from Greek: $\kappa\alpha\tau\alpha$, 'down', and $\lambda\upsilon\epsilon\iota\nu$, 'loosen'),[3] coined by the Swedish chemist Jöns Jacob Berzelius 40 years later.[4] Catalysis has since then grown to an important chemical field. An important point in history was the invention of the Haber–Bosch process – synthesis of ammonia (NH_3) from hydrogen and nitrogen with an iron catalyst – in the beginning of the 20th century.[5–7] The new, effective method of producing artificial fertiliser revolutionalised global agriculture, allowing for a population growth from 1.6 billion in 1900 to 7 billion today. Catalysis has proven useful for a number of other processes in the chemical industry; crude oil is catalytically cracked to shorter carbon chains, e.g. gasoline, with the help of zeolites.[8]; selective oxidation of ethylene to ethylene epoxide is carried out directly using a silver catalyst, instead of an earlier multi-step process requiring chlorine gas.[9] As concerns for health and environment have increased towards the later part of the 20th century, catalytic processes for exhaust treatment have been developed. Examples of these are NO_x reduction[10] and CO oxidation[11, 12] in combustion engines.

Another modern application is energy conversion and storage, such as batteries and fuel cells, which belong to a certain class of catalysis involving electrochemistry. Electrochemistry is the relationship between chemical and electrical energy, which can be understood by describing the electrochemical cell (Figure 1.1).[13] This consists typically of two solid electrodes, the anode and the cathode, connected to each other via a power source or load and an electrolyte. The electrolyte is normally liquid and its purpose is to conduct ions between the electrode. The electrons, on the other hand, pass through the wire from the anode to the cathode giving rise to or being driven by a potential. The reaction, including charge transfer, takes place at the surface of the electrode. As long as the electrode is not consumed, it is a catalyst by definition. To stress the catalytic nature of the process, the term *electrocatalysis* was used by Kobozev and Monblanova in the 1930s when studying the kinetics of the hydrogen evolution reaction (HER)[14][1], where protons and electrons combine to form hydrogen gas,

$$2\,H^+ + 2\,e^- \longrightarrow H_2, \tag{1.1}$$

[1] To the best of my knowledge, the term is coined in this paper.

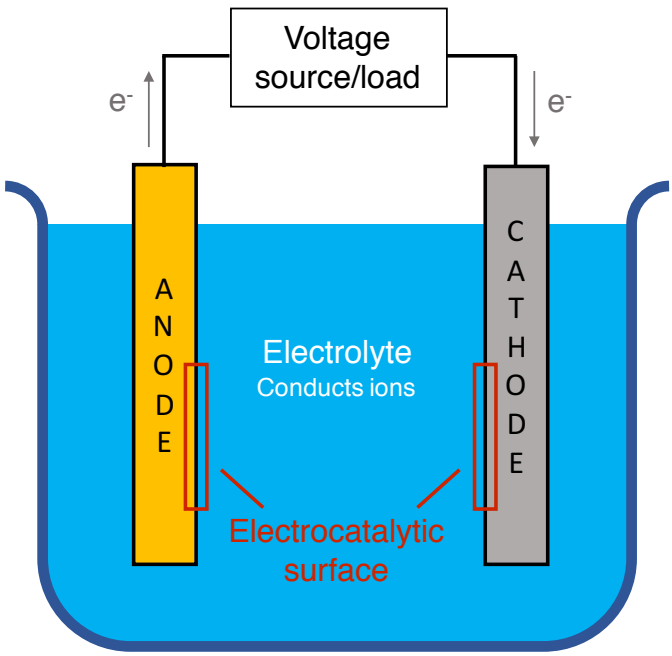

Figure 1.1: Sketch of a simple electrochemical cell. The electrons travel from the anode to the cathode in via a voltage source (electrolytic cell) or a load (galvanic cell). Charged ions are moving through the electrolyte to charge compensate. The reactions occur on the electrode surfaces, which acts as catalysts in the sense that they can be more or less effective at facilitating the electrochemical reactions.

on different metals. It should be pointed out that electrocatalysis is not really a subcategory of electrochemistry; there is no zero-activity electrode, and thus no non-catalysed reaction. Electrocatalysis refers to relative catalytic properties of possible electrode materials.[13]

1.1 Motivation

Today, most of the fuel needs in the world are met with fossil sources.[15, 16] The use of fossil fuels leads to emission of CO_2 in the atmosphere, which have been shown to cause global warming.[17, 18] The climate change, being rapid in a geological perspective, is devastating to slowly-adapting ecosystems[19] and to human civilisation.[20, 21] In order to decrease CO_2 emissions, we need to replace oil, coal, and gas with sustainable sources of energy. Alternative fuel solutions are fuel cells and batteries, as mentioned above, to which biodiesel can be added. Biodiesel is produced via esterification of fatty acids from vegetable oils and animal fats. Millions of metric tonnes of glycerol is produced annually as a byproduct in this process. Glycerol is not particularly useful as it is, but it can be converted to more valuable products. Using electrooxidation, we can produce H_2 and derivatives such as dihydroxyacetone, glyceraldehyde, glyceric acid. We could also imagining go all the way to CO and then use water-gas shift, $CO + H_2O \longrightarrow H_2 + CO_2$, to produce even more H_2. H_2 has a wide range of applications, such as fuel cells, upgrading biofuels via hydrogenation of unsaturated fatty methyl esters,[22] or steel production, which is tested in Sweden.[23] The other derivatives are somewhat interesting, but not in the same scale.

Methanol electrooxidation can be seen as a prototypical reaction, used for benchmarking and as a model system for glycerol. In addition, methanol can be used in direct methanol fuel cells to generate electricity, which has grown in interest recently.[24]

1.2 Scope

The aim of this thesis is to use electronic structure calculations, supported by experimental verification, to study reaction conditions and mechanisms for glycerol and methanol electrooxidation on gold. The calculations, performed with density functional theory, is used to determine adsorption energies, reaction intermediates and paths, vibration energies, potential-dependent surface conditions, and theoretical onset potentials. We investigate the impact of microsolvation and long range dispersion. The work is restricted to thermodynamics, excluding calculations on kinetics and transport processes.

To do this, we start by discussing the theory of electrocatalysis in Chapter 2, leading up to understanding how to construct a suitable computational model. Chapter 3 outlines density functional theory, an application of quantum mechanics to calculate energies of atomic systems. In order to use these energies to calculate measurable properties such as vibration frequencies and reaction free energies, we discuss e.g. vibrational analysis and semi-classical thermodynamics in Chapter 4. A summary of the important results of the papers, followed by discussion and outlook, is given in Chapter 5.

Chapter 2

Electrocatalysis

> “
> Let us now analyse the situation for natural forms of diffusion, occlusion and catalysis, where the first step is always the ‘natural’ adsorption of the component, and their ‘forced’ form, e.g. electroocclusion, electrodiffusion or electrocatalysis, where H atoms are forcibly formed in the final state at the membrane by the electrical current.
>
> – Nikolai Ivanovich Kobozev and Valentina Viktorovna Monblanova [14]

As we have seen from the historical overview, electrocatalysis has emerged as a cross-disciplinary field between electrochemistry and catalysis. To introduce this field, we discuss catalysis and electrochemistry separately.

2.1 Catalysis

Let us assume that we have an non-catalysed reaction in gas phase with reactants A and B and the product P,[9]

$$\mathrm{A} + \mathrm{B} \longrightarrow \mathrm{P}. \tag{2.1}$$

We assume that the reaction occurs in one step, which is justified at the timescales we are interested in. A prerequisite for the reaction is that the reactants are in contact. This means that we can expect the rate r to be proportional to the partial pressures p_i,

$$r_+ = p_\mathrm{A} p_\mathrm{B} k_+ \tag{2.2}$$

where k_+ is the rate constant, and the plus denotes the forward reaction (from left to right in Equation 2.1). The reactants need to overcome an energy barrier, corresponding to breaking and forming chemical bonds. The energy required to overcome the barrier is called *activation energy*, E_A, and must in this case come from the kinetic energy of the molecules. At any given temperature, T, there is a distribution of kinetic energy among the molecules such that a portion of them can overcome E_A. As the average kinetic energy increases linearly with temperature, it can be argued that the rate constant should be

$$k_+ = A_+ e^{-\beta E_A}, \tag{2.3}$$

where A_+ the concentration-dependent preexponential and $\beta = \frac{1}{k_\mathrm{B} T}$, where k_B is the Boltzmann constant. Svante Arrhenius proposed this equation in 1889,[25, 26] and a similar result was derived from collision theory 27 years later.[27] The Arrhenius equation governs the *kinetics* of the reaction, i.e. the rate over reaction barriers. This is in contrast

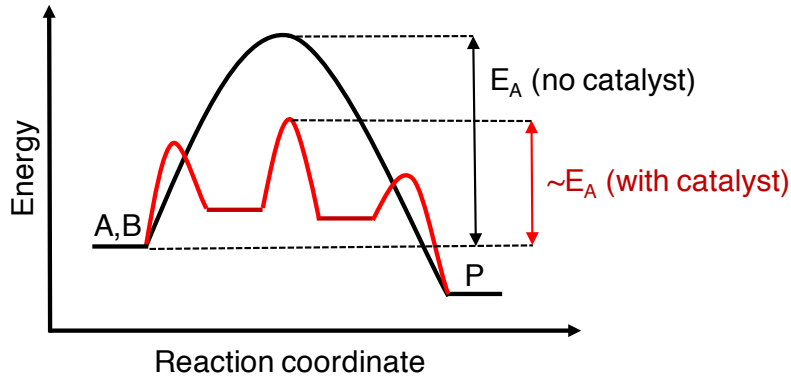

Figure 2.1: The effect of a catalyst in terms of energy barriers. The uncatalysed reaction (black) has fewer intermediate steps and can often be modelled as a single reaction associated with a single energy barrier. The catalyst introduces more intermediates with lower barriers (red), giving a lower effective barrier for the reaction. The figure adapted from Wikimedia Commons.[28]

with the macroscopic reaction rate, the *activity* (not to be confused with thermodynamic activity), which might be influenced by e.g. transport limitations.[9]

In the presence of a catalyst, reactants will form bonds to it via its *active site*, while loosening their own intramolecular bonds. In addition to an easier bond breaking, the catalyst allows the formation of intermediates. This means that the catalysed reaction can have several steps, each associated with a smaller reaction barrier compared to the fewer ones (possibly a single one) in gas-phase (Figure 2.1).[9]

A catalyst can not alter the thermodynamics of the total reaction, just introduce stepping stones. However, it is possible that the formation of another product, Q, is thermodynamically favourable, but the kinetics of this reaction is inferior to formation of P. By choice of a suitable catalyst, it is possible to make the new kinetics favour Q to P. This property, shown in Figure 2.2, is called *selectivity*.[9]

In order for a catalytic reaction to occur, the reactants, intermediates and products must not bind too strongly nor too weakly to the catalyst. If they adsorb too weakly, they will not be able to adsorb or react on the surface. If they bind to strong, they will break the catalytic cycle and physically block new reactants from reaching the surface (*poisoning* the surface). This is called the *Sabatier principle*.[29] Assuming that adsorption and desorption are governing the reaction rate, the catalytic rate can be plotted as a function of bond strength limited by two linear equations, corresponding to adsorption and desorption limitation, respectively. To these two, constraints related to reaction thermodynamics and kinetics can be added. Such a plot, as seen in Figure 2.3, may often be referred to as a *volcano plot* because of this shape.[9]

Since a catalyst is not consumed, by definition, it should have infinite lifetime. In practice, catalysts deactivate over time for a number of reasons.[30] These can be more related to the reaction, such as poisoning the active sites by intermediates or byproducts, or

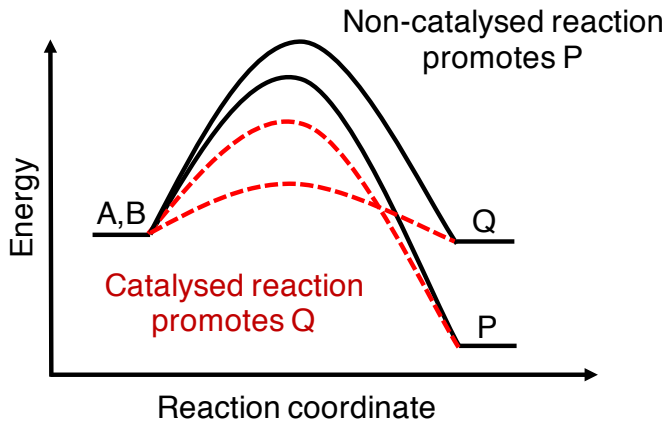

Figure 2.2: Example of a catalyst changing its selectivity from product P to product Q by altering the relative barrier heights. Non-catalysed reaction in black and catalysed in red.

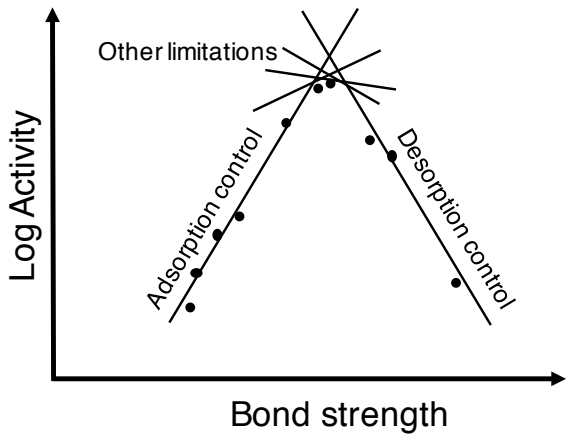

Figure 2.3: The Sabatier principle as a volcano plot. The catalytic activity is limited by bond strength to reactants and products. The highest activity is obtained with a catalyst that neither binds to strongly or to weakly to the adsorbents. There are other thermodynamic and kinetic limitations, which can have impact when the optimal bond strength is achieved.

physically blocking the surface (fouling). Processes can also decrease the surface area, e.g. by changing the surface composition, or coalescing smaller particles to larger (sintering). It is also possible for the surface to suffer mass loss. Thus, the *stability* is an important property for a real catalyst.[9] Stability in electrocatalysis differs from other branches of catalysis, since it is the potential that makes the system reactive, while temperature and pressure are relatively low (limited by the normally aquatic environment).

There are three large classes of catalysis – biocatalysis, homogeneous catalysis and heterogeneous catalysis.[9] Biocatalysts, i.e. enzymes protein synthesis, uses its geometric structure to facilitate a reaction. Homogeneous and heterogeneous catalysts typically have a more specific active site, consisting of few or single atoms; the difference them lies in the phases of the catalyst and the reactants. In homogeneous catalysis, they are in the same phase, typically liquid phase. In heterogeneous catalysis, the catalyst is in one phase (typically solid) and reactant are in a different phase (gas or liquid). Electrocatalysis falls within the latter category, since the reactants are dissolved in the electrolyte and the catalytically active electrodes are solid.

2.2 Electrochemistry

Electrochemical reactions are chemical processes that involve charge transfer across an interface between a solid and a liquid phase.[13] Electric potential can be used to drive the reaction, which is called electrolysis, e.g. splitting of water to hydrogen and oxygen and glycerol and methanol electrooxidation. Alternatively, electric power can also be generated by the reaction, which is the case in a galvanic cell, e.g. batteries, and metal corrosion.

The electrochemical cell, as described in the introduction and shown in Figure 1.1, has two electrodes connected with wires conducting electrons and an electrolyte conducting ions – the anode and the cathode. Reduction reactions (where electrons are gained) occur at the cathode, and oxidation reactions (where electrons are lost) occur at the anode[1]. The pair of reactions are called half reactions, since they must occur simultaneously due to charge conservation. As an example, we have water splitting, where the cathodic half reaction is HER,

$$2\,\mathrm{H^+} + 2\,\mathrm{e^-} \longrightarrow \mathrm{H_2} \tag{2.4}$$

and the anodic reaction reaction is the oxygen evolution reaction (OER)

$$\mathrm{H_2O} \longrightarrow 2\,\mathrm{H^+} + 2\,\mathrm{e^-} + \frac{1}{2}\mathrm{O_2} \tag{2.5}$$

with the total reaction

$$2\,\mathrm{H_2O} \longrightarrow 2\,\mathrm{H_2} + \mathrm{O_2}. \tag{2.6}$$

The anode and cathode half reactions can in many respects be treated separately. For example, the products from water splitting, $\mathrm{H_2}$ and $\mathrm{O_2}$, can be collected without mixing

[1] There is a misconception that the anode is always at a higher potential than the cathode. This is true for an electrolytic cell, but it is the opposite in a galvanic cell. In both cases, the electrons flow from the anode to the cathode, but in the galvanic case spontaneously (towards the positive cathode) and in the electrolytic case forcibly.

at the cathode and anode respectively. This is a general and practical feature for electrochemical reactions.

2.2.1 Nernst equation

We consider the total electrochemical reaction to occur in an isothermal-isobaric ensemble with constant temperature T, pressure p and number of particles N. The thermodynamical potential in this ensemble is the Gibbs free energy, G, with differential

$$\mathrm{d}G = V\,\mathrm{d}p - S\,\mathrm{d}T - \mathrm{d}W_{\mathrm{el}} \tag{2.7}$$

where V is the volume, S the entropy and W_{el} the electric work.[31] Since the pressure and temperature are constant, we see that the difference in Gibbs free energy equals the electric work. The work can be simply derived as the energy gained or lost by moving n_e electrons with charge e over the electric potential U measured vs. a U_{ref},[13] meaning that

$$\Delta G = -n_e e U. \tag{2.8}$$

The Gibbs free energy for species i in a mixture is dependent on the thermodynamic activity a

$$G_i = G_i^0 + k_{\mathrm{B}} T \ln a_i \tag{2.9}$$

where the superscript 0 denotes a standard state.[13] The activity can be seen as an 'effective concentration'; in the dilute limit, they are equal, but with increasing concentration, the interactions between the particles lowers their ability to be chemically active. In practical calculations, the activity is commonly approximated by properly normalised concentrations.

Inserting Equation 2.8 in Equation 2.9 gives

$$U_i = U_i^0 + \frac{k_{\mathrm{B}} T}{n_e e} \ln a_i \tag{2.10}$$

which is known as the Nernst equation.[32] In principle, U_i can be defined anywhere in the cell, but it turns out that it is only possible to measure the potentials of the metal electrodes, and only relative to a standard electrode.

2.2.2 The double layer

Naively, one might think that the potential drops linearly through the electrolyte. However, it turns out that almost the entire potential drop occurs close to the electrodes in the thin *double layer*.[13] The name refers to the fact that there is one charged layer in the electrode surface and an opposite charge layer in the adjacent electrolyte, which effectively screens the rest of the cell (Figure 2.4). As the thickness of the layer in the electrolyte is in the order of magnitude of the size of hydrated ions, the local electric field is large. From a modelling perspective, this means that the local properties of the double layer, e.g. the electric constant of water,[33] are hard to determine and can not be expected to be similar to the ones in the bulk solution.

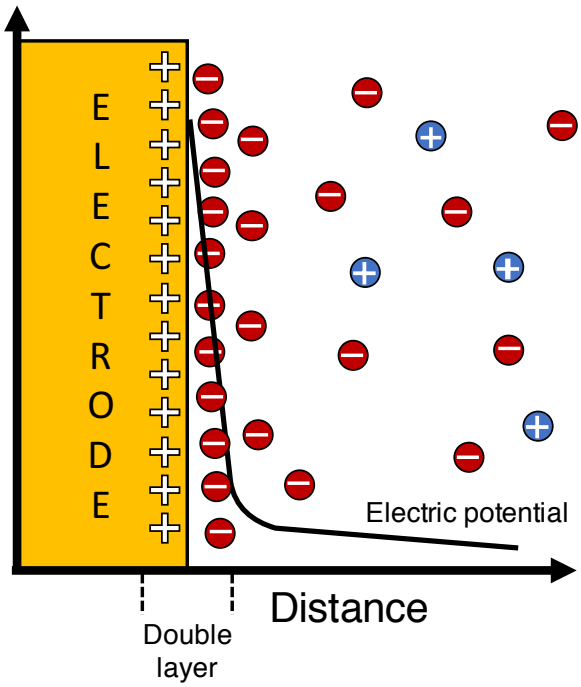

Figure 2.4: The potential difference between the electrode and the electrolyte forms a layer of opposite charges, the double layer, in each medium at the interface. This screens the electric potential effectively, so that almost the entire potential drop takes place there.The figure adapted from Wikimedia Commons.[34]

On a more macroscopic level, the double layer can be seen as a plate capacitor with a differential capacitance

$$C_d = \frac{\mathrm{d}Q}{\mathrm{d}U} \tag{2.11}$$

where Q is the charge in either of the layers and U is the potential between the electrode and the electrolyte.[13] In an experiment where the potential is varied, (i.e. cyclic voltammetry, section 2.3), a current is generated from the charging and discharging of the double layer.

2.2.3 Reference electrodes

Experimentally, it is desirable to keep track of the electric potential. It is impossible to measure the potential difference between an electrode and the electrolyte, since the insertion of a conducting device would introduce a new phase barrier and a new double layer.[13] However, it is possible to measure the relative potential between electrodes. By using a known equilibrium equation, it is possible to construct a reference electrode. All reactions can then be defined relative to the reference.

Historically, the normal hydrogen electrode (NHE) have been used as a reference potential, defined as the equilibrium for hydrogen gas and free protons and electrons

$$\mathrm{H_2} \longleftrightarrow 2\,\mathrm{H^+} + 2\,\mathrm{e^-}, \tag{2.12}$$

on platinum in a 1 N acid solution (i.e. 1 M $\mathrm{H^+}$ or pH 0) at 1 atm and 298 K.[35] The reason for this definition is that it is easy to construct such an electrode in practice. Later, it has been viewed as more suitable to have a reference where the thermodynamic activity of the hydrogen ions is 1 (i.e. they do not interact with other ions). The latter is known as the standard hydrogen electrode (SHE).[2] Such an electrode can not be constructed, but it can be used as basis for tables on electrodes.

When hydrogen evolution or oxidation half reactions (Equation 2.12) are involved in the total reaction, the electrode potential depends on pH, since hydrogen concentration is included in the Nernst equation. The potential shift,

$$\Delta U = -\frac{k_\mathrm{B}T}{e}\ln[\mathrm{H^+}] = +\frac{k_\mathrm{B}T}{e\ln 10}\mathrm{pH} \tag{2.13}$$

may be included in the potential itself,[3] which defines the reversible hydrogen electrode (RHE),[36]

$$U_\mathrm{RHE} = U_\mathrm{SHE} + \frac{k_\mathrm{B}T}{e\ln 10}\mathrm{pH}. \tag{2.14}$$

2.2.4 Kinetics

Consider the Arrhenius equation for the backward and forward rates of an equation with only one step,[13, 37]

$$r = r_+ - r_- = A_+ c_\mathrm{reac.} e^{-\beta G_{A,+}} - A_- c_\mathrm{prod.} e^{-\beta G_{A,-}}. \tag{2.15}$$

The current i, as well as the forward and backward currents i_+ and i_-, are proportional to the rates with a factor $n_e e$. At the equilibrium potential, U_0, the forward and backward currents are equal. The exchange current density, i_0 is defined as this current,

$$i_0 = i_+(U_0) = i_-(U_0). \tag{2.16}$$

At other potentials there will be a net current in either direction. We define the overpotential[4]

$$\eta = U - U_0. \tag{2.17}$$

Remember that the thermodynamics of the initial and final states of the reaction changes linearly with the electric potential. This change, $\Delta G = -n_e e\eta$, is added to the difference between the reaction barriers, see Figure 2.5. We introduce a transfer coefficient, $0 \leq \alpha \leq 1$

[2] SHE also differs from NHE that the former is defined at 1 bar = 10^5 Pa, slighly lower than 1 atm, but this is generally negligible.

[3] At room temperature, this shift is 0.059 V per pH.

[4] The term overpotential is sometimes colloquially used for the limiting potential relative to the equilibrium potential, see below.

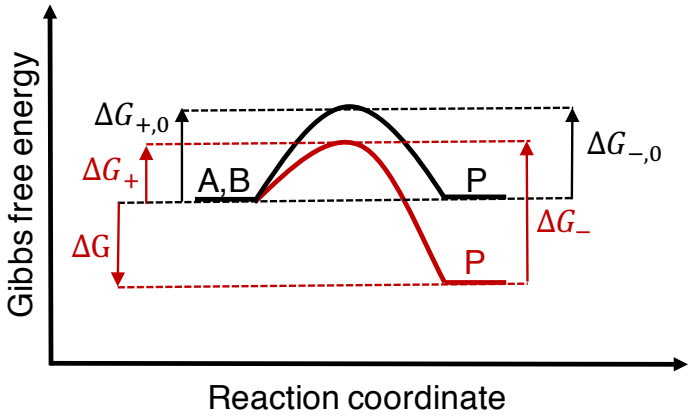

Figure 2.5: Energy landscape of a reaction at the equilibrium potential (black) and a more oxidative potential (red). The change in Gibbs free energy, ΔG, is equal to the barrier difference, $\Delta G_+ - \Delta G_-$.

such that

$$\Delta G_+ = \Delta G_{+,0} - \alpha n_e e \eta \tag{2.18}$$

and

$$\Delta G_- = \Delta G_{-,0} + (1-\alpha) n_e e \eta. \tag{2.19}$$

Thus we have an expression for the total current,

$$i = i_0 \left(e^{\alpha \beta n_e e \eta} - e^{-(1-\alpha)\beta n_e e \eta} \right) \tag{2.20}$$

which is known as the the Butler-Volmer equation. When going to overpotentials far from 0, and as long as the reaction is not limited by transport processes, one of the terms can be neglected, which gives a linear relationship with the logarithm of the current,

$$\eta = b(\ln i - \ln i_0) \tag{2.21}$$

where

$$b = (\alpha \beta n_e e)^{-1} \tag{2.22}$$

is called the Tafel slope.

We see that the thermodynamic landscape – both the product/reactant energies and the barriers – depend strongly on the potential. This is a difference vis-à-vis kinetics in standard catalysis, where we normally treat the barriers as independent of the temperature. A potential is a far superior driving 'force' compared to temperature – a potential of 0.5 eV corresponds to the thermal energy at 6000 K.

Multi-step reactions

Consider an electrochemical reaction with several steps and let us say that it is an oxidation. At the equilibrium potential between the reactants and the products, U_0,

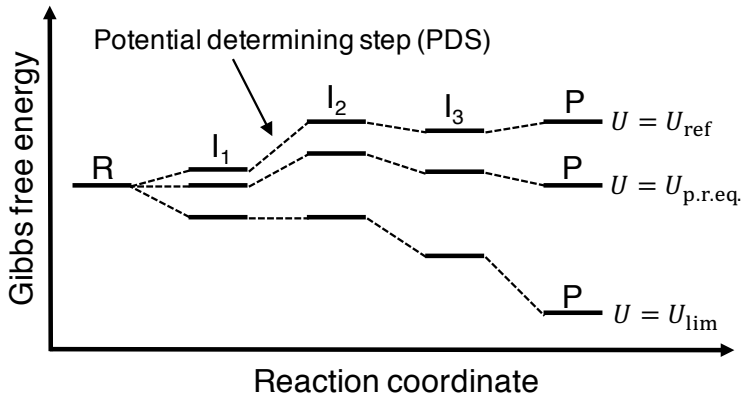

Figure 2.6: Energy landscape of a reaction with four elementary one-electron transfer steps (corresponding to three intermediates). At the reference potential, U_{ref}, some of these steps are uphill and the reaction is not thermodynamically favourable. The largest of these is identified as the PDS. At the product-reactant equilibrium potential $U_{\mathrm{p.r.eq}}$, there are typically still uphill steps, including the PDS. At the theoretical limiting potential, U_{lim}, the PDS is at equilibrium and the reaction is spontaneous. We have $\Delta G_{\mathrm{PDS}} = eU_{\mathrm{lim}}$.

there are generally intermediates with lower and higher energy. If we want the forward reaction to be spontaneous, we need to increase the potential until the highest step is energetically 'levelled out', see Figure 2.6. This step is called the *potential determining step* (PDS)[38] and we refer to the associated potential as the *theoretical limiting potential*,[5] U_{onset}.[39] A reaction with several steps has coupled Butler-Volmer equations for every step. Above the theoretical limiting potential, the current is expected to increase more or less exponentially in the kinetic regime. If the PDS is significantly higher than other steps, it can be considered rate-determining, and then the Tafel slope could be associated with it. Regardless, it is not straightforward to find a precise onset potential.

There are three common ways of defining an experimental onset potential,[40] as illustrated in Figure 2.7:

a) The potential at which the current exceeds a critical value, i_{crit}.

b) The potential at which the slope, $\mathrm{d}j/\,\mathrm{d}U$ exceeds a critical value.

c) The potential at which the tangent to the curve at the maximum slope of $i(U)$ intersects $i = 0$.

None of them rests rigorously on theoretical foundations. In this project, we are trying to verify calculated limiting potentials, so the important concern is to choose a definition that corresponds to potential where thermodynamics becomes favourable, i.e. the definition of the theoretical limiting potential shown in Figure 2.6. Still, we should keep in mind that an experimental onset potential is not an exact value.

[5] We refer to it as theoretical onset potential in **Paper II**.

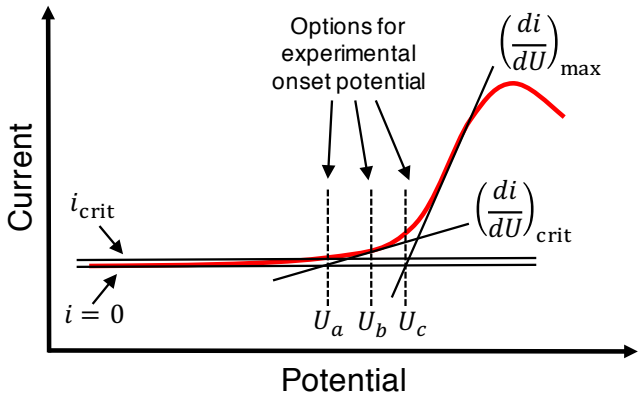

Figure 2.7: Three ways of defining experimental onset potential. a) Critical current. b) Critical slope. c) Tangent intersection. The choice of critical current and critical slope are in principle arbitrary, as long as chosen within reason.

Since the focus of this thesis is thermodynamics, only currents near the onset potential are of interest. Thus we can neglect transport processes from this discussion.

2.3 Cyclic voltammetry

Cyclic voltammetry (CV) is a measurement technique, where the potential in an electrochemical cell is varied forward and back between two potentials, and the current is measured as output.[13, 41] Figure 2.8 shows a schematic CV setup with three electrodes – a working electrode (WE), a counter electrode (CE) and a reference electrode (RE)[6] – connected to a potentiostat, operating as an adjustable power source, a voltmeter, and an ammeter. The source potential, U_s, is applied between the WE and CE. The potential between the WE and the RE, U_m, is measured with the voltmeter, and is kept at the desired potential variation by adjusting U_s. The current between the WE and the CE is measured with the ammeter. The setup allows the study of the WE only, since the circuit with the RE and the CE makes sure that U_s is large enough, regardless of the choice of CE. In order to study oxidation reactions on gold, a polycrystalline gold WE was used. The cell setup, including a graphite CE and a Ag/AgCl RE, can be seen in Figure 2.9.

We are interested in converting the measured electrode potential to a standard electrode. Since the studied reactions in this work are pH dependent, we choose RHE. The conversion is carried out with the help of the Nernst equation,

$$V_{\text{RHE}} = V_{\text{AgCl},0} + \frac{k_{\text{B}}T}{e}\left(\ln c_{\text{KCl}} c_{\text{reac.}} + \frac{\text{pH}}{\ln 10}\right) \tag{2.23}$$

[6]The reason for terminology is that the working and counter electrodes typically alternate between being anode and cathode, as the potential is changing.

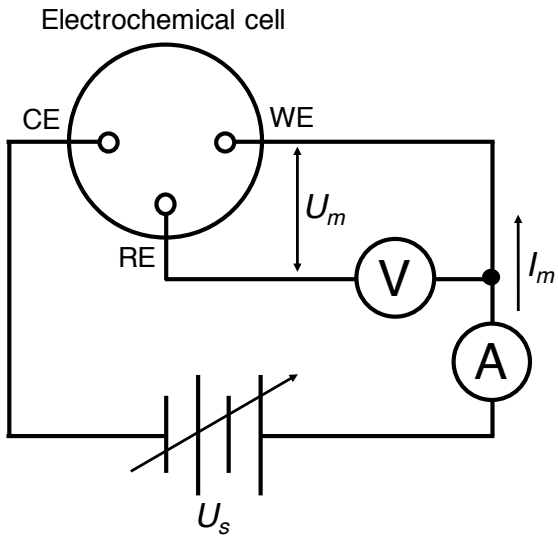

Figure 2.8: Circuit diagram for basic cyclic voltammetry. Adapted from SJ Electronics.[41]

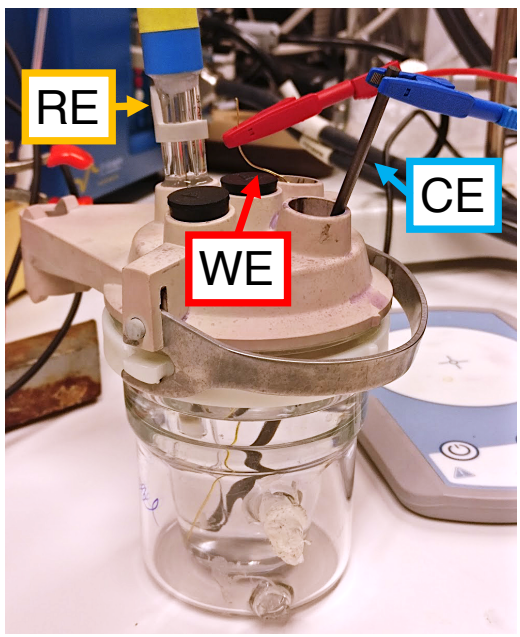

Figure 2.9: Setup of electrochemical cell for cyclic voltammetry. The working electrode (WE) is a polycrystalline gold wire, the counter electrode (CE) a graphite rod, and the reference electrode (RE) Ag/AgCl.

where c_{KCl} is the concentration of KCl in the reference electrode and $c_{\mathrm{reac.}}$ the concentration of (oxidative) reactant, such as glycerol or methanol.

The accuracy of the potentiostat is generally high, in terms of control and sensitivity. However, CV provides no direct information about the cause of the currents. In order to interpret a voltammogram, one must be able to recognise features that are not directly related to the studied reaction. Hydrogen evolution starts when going to low (cathodic) potentials and oxygen evolution (OER) starts when going to high (anodic) ones; on gold, HER starts around the equilibrium potential 0 V vs. RHE[42] while OER requires around 0.7 V of overpotential above the equilibrium potential of 1.23 V vs. RHE.[43] Dissolved atmospheric oxygen is reduced below 1.23 V, according to the oxygen reduction reaction (ORR, the backward reaction in equation 2.5), which can be prevented by purging the cell with nitrogen or argon. There will be a latent current, positive on the anodic scan and negative on the cathodic scan, corresponding to the capacitive properties of the double layer. Surface oxidation/reduction can also be seen.

In order to try to single out the desired reaction, two runs are usually performed – one with the reactant and one without – to study the difference between them. Still, only the current is obtained and the mechanism and the products remain unknown.

There are several possible methods to measure the products. Gas chromatography (GC) and high performance liquid chromatography (HPLC) are methods for separating gas and liquid products respectively,[44] which are followed by detection processes. While such analysis could be interesting in the future, we have considered it to be out of scope for this mostly theoretical project.

2.3.1 Underpotential deposition of copper (Cu UPD)

CV gives a total current, but we are generally more interested in surface current density. This requires us to know the electrochemically active area of the electrode submerged in the electrolyte. This can be done with underpotential deposition of Cu (Cu UPD).[45]

The equilibrium potential for the reaction

$$\mathrm{Cu} \longleftrightarrow \mathrm{Cu}^{2+} + 2\,\mathrm{e}^- \tag{2.24}$$

is 0.34 V vs. RHE,[13] meaning that Cu ions in the solution will reduce and form metallic Cu in bulk below this potential. However, it is possible to form a monolayer of Cu at a slightly higher potential. Ideally, a cathodic scan will see two distinguished reduction peaks corresponding to these two processes. The total charge of one monolayer of Cu is computed by integration of the first peak (Figure 2.10). The charge can be converted to a surface area, given knowledge of the surface facets.[45]

2.4 Modelling electrocatalysis

We now approach the main task of modelling electrocatalysis on an atomic level. This is not an easy task due to four reasons:

- The double layer, where the reaction occur, has a strong electric field; its properties, like dielectric constant of water or pH, are very different from the properties of

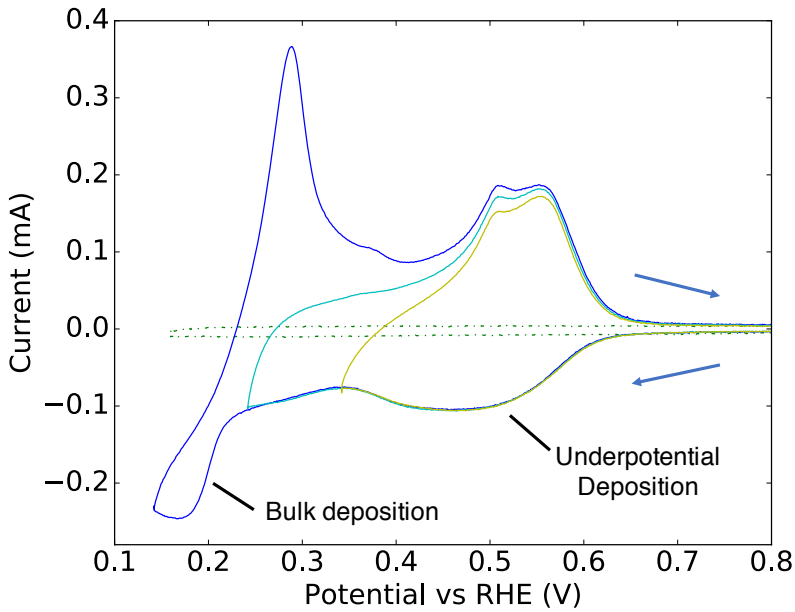

Figure 2.10: Underpotential deposition of copper from supporting information to **Paper II**. As the potential is decreased, a monolayer of Cu forms on the Au surface. Eventually, bulk Cu is deposited (blue). By turning the potential sweep before the bulk deposition (cyan, yellow or somewhere in between), we can measure the deposited and released charge q_{ML} to calculate the surface area. The dotted line is the blank run, dominated by capacitive effects of the double layer.

the bulk of the solvent and depend heavily on small displacements relative to the electrode.[33, 46]

- Varying electric potential changes the thermodynamic landscape, including barriers. Even if it would be possible to calculate a barrier, it does not mean that it is valid at different potentials.
- The proton and electron transfer are hard to model, since it is not conclusively known how the processes takes place.[47]
- It turns out that electron structure calculations in a system with periodic boundary conditions has difficulties with handling charged systems.[48]

2.4.1 Computational hydrogen electrode

We know that 0 V vs. RHE is the equilibrium potential for hydrogen protolysis by definition. This means that these systems have the same Gibbs free energy at standard conditions. We also know that the electric energy of the electron is eU. If we now assume that G_{H_2} is independent of the potential, we can calculate the energy of the protolysed system by running an electronic structure calculation for H_2 and then just add the eU term, visualised in Figure 2.11. This is known as the computational hydrogen electrode (CHE).[49, 50] In order to use it in calculations with other species, we need to assume that the energy of neutral species (including H_2) are independent of the potential.

The CHE is an elegant way of avoiding some of the problems of electrochemical modelling. There are, however, a number of limitations of the model:

- It assumes that everything except H^+ and e^- are independent of potential (and electric field). This can break down, in particular for large molecules that extend beyond the double layer into the electrolyte, since there will be a large potential gradient over the molecule.
- It assumes that electron-proton transfer is coupled, which is not necessarily always the case.
- Barriers and kinetics can not be modelled, since the model circumvents them.

More complex models

There have been further model development to directly model the double layer and kinetics. By introducing a multilayer of water and hydrogen atoms, electrons will be transferred from the hydrogen atoms to the surface. The potential can be regulated by the number of hydrogen atoms, which requires a large simulation cell to sample the potential range. Kinetics with coupled electron-proton transfer can be modelled, but the potential will vary throughout the thermodynamic barrier, again requiring a large simulation cell to diminish the effect.[51, 52]

Alternative models try keep the potential constant by changing the charge. These include explicit charging the surface, compensating with a homogeneous background[53]

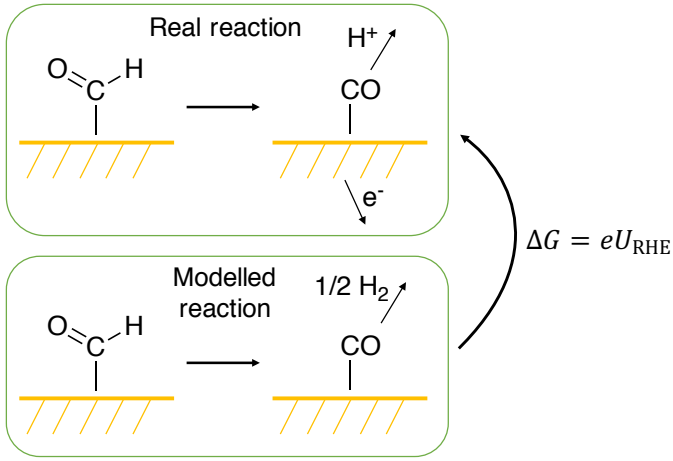

Figure 2.11: Computational hydrogen electrode.

or jellium (uniform electron gas) in the electrolyte region,[54] and implicitly compensating for energy corresponding to potential change (assuming that it is separable)[55],

2.4.2 Surface Pourbaix diagrams

A Pourbaix diagram is a two-dimensional phase diagram as a function of pH and potential,[13] named after Marcel Pourbaix for his studies of corrosion. The diagram is calculated using thermodynamic data of the material in question and the Nernst equation. However, the diagrams that use tabulated experimental data is normally only valid for the bulk of the material, and we are interested in knowing the local surface structure. Using density functional theory, it is possible to construct a surface Pourbaix diagram by calculating the energy of adsorbed oxo (*O) or hydroxo (*OH) groups.[56] The surface Pourbaix diagram is easy to read since it is one-dimensional, only depending on the potential, since the pH dependence is implicit when using RHE (Figure 2.12).

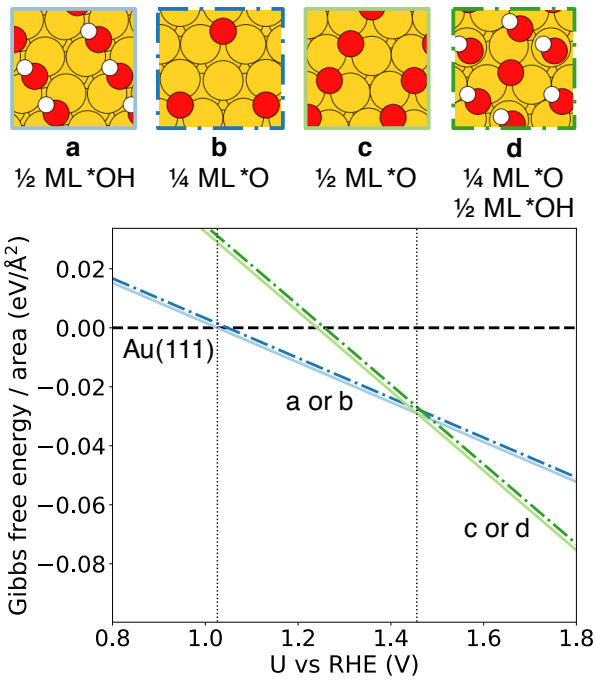

Figure 2.12: Surface Pourbaix diagram of Au(111) calculated in **Paper II**. The surface is adsorbent-free at potentials below 1.0 V vs. RHE, above which (a) 1/2 ML *OH and (b) 1/4 ML *O are formed. At 1.5 V, (c) 1/2 ML *O and (d) a mixture of 1/4 ML *O and 1/2 ML *OH are formed.

Chapter 3

Density functional theory

> “
> The underlying physical laws necessary for the mathematical theory of a large part of physics and the whole of chemistry are thus completely known, and the difficulty is only that the exact application of these laws leads to equations much too complicated to be soluble.
>
> – Paul Dirac [57]

3.1 From Dirac to Schrödinger

We start our derivation from a relativistic regime (see Strange[58] for further details). The behaviour of quantum mechanical systems is governed by the time-dependent Dirac equation

$$i\hbar\frac{\partial}{\partial t}\Phi(\mathbf{r},t) = \hat{H}\Phi(\mathbf{r},t). \tag{3.1}$$

where the Hamiltonian $\hat{H}$ is a system-dependent operator with real eigenvalues (normally Hermitian), and $\Phi(\mathbf{r},t)$ is the wavefunction, containing all information about the quantum mechanical system.[59] By separation of variables, we assume that the wavefunction can be written as a product of purely time-dependent and a space-dependent parts,

$$\Phi(\mathbf{r},t) = \Psi(\mathbf{r})\chi(t), \tag{3.2}$$

which inserted in equation 3.1 gives

$$\frac{i\hbar}{\chi(t)}\frac{d\chi(t)}{dt} = \frac{1}{\Psi(\mathbf{r})}\hat{H}\Psi(\mathbf{r}). \tag{3.3}$$

As both sides depend only either time or space, they must be constant. It turns out that this constant is the energy, E, so that the time-dependent part, χ can be solved as

$$\chi = e^{\frac{-iEt}{\hbar}} \tag{3.4}$$

and the space-dependent part, Ψ must obey the time-independent Dirac equation,

$$\hat{H}\Psi = E\Psi. \tag{3.5}$$

As we can see, the energies are the eigenvalues of the Hamiltonian. The classical expression of relativistic energy is

$$E = \sqrt{p^2c^2 + m^2c^4}, \tag{3.6}$$

and by insertion of the quantum mechanical operators for momentum, $\hat{\mathbf{p}} = -i\hbar\nabla$, we get the following equation

$$c(-i\boldsymbol{\alpha}\cdot\nabla + \beta mc)\Psi(\mathbf{r}) = E\Psi(\mathbf{r}). \tag{3.7}$$

In order for the square of the right hand side to be equal to the square of the energy, the cross terms must be zero. This means that α and β must be 4×4 matrices, constructed as blocks of 2×2 Pauli matrices and identity matrices. Thus, $\Psi(\mathbf{r})$ is a four-component wavefunction. These four terms correspond to a pair of 2×2-spinors. By rewriting the Dirac equation in the presence of an electromagnetic field, it can be seen that one of the spinors is an order of c smaller than the other one.[1] In the non-relativistic limit, the smaller spinor may be eliminated, and by shifting the the absolute energy with mc^2, we get the (time-independent) Pauli equation,

$$\Big(\frac{1}{2m}\big(-i\hbar\nabla - e\mathbf{A}(\mathbf{r})\big)^2 - \frac{e\hbar}{2m}\boldsymbol{\sigma}\cdot\hat{\boldsymbol{B}}(\mathbf{r}) + V(\mathbf{r})\Big)\Phi(\mathbf{r}) = E\Psi(\mathbf{r}) \tag{3.8}$$

The two components of the wavefunction correspond to spin up and down and are coupled via the magnetic field term. In the absence of magnetic field, the two spin states are no longer coupled and we can reduce the wavefunction to one component. We end up with the familiar time-dependent Schrödinger equation.

$$\Big(-\frac{\hbar^2}{2m}\nabla^2 + V\Big)\Psi = E\Psi. \tag{3.9}$$

3.2 The many-body problem

We are considering a system consisting of N electrons with charge e and K positively charged nuclei with charge $Z_I e$. As the potential between two particles with charges q_1 and q_1 is given by the Coulomb interaction

$$V(r) = \frac{q_1 q_2}{4\pi\epsilon_0 r} \tag{3.10}$$

we can write the Hamiltonian as [60, 61]

$$\begin{aligned}\hat{H} = &-\sum_{i=1}^{N}\frac{\hbar^2}{2m_\mathrm{e}}\nabla_i^2 - \sum_{I=1}^{K}\frac{\hbar^2}{2M_I}\nabla_I^2 + \frac{1}{4\pi\epsilon_0}\sum_{i=1}^{N}\sum_{j>i}^{N}\frac{e^2}{|\mathbf{r}_i-\mathbf{r}_j|}\\ &-\frac{1}{4\pi\epsilon_0}\sum_{I=1}^{K}\sum_{i=1}^{N}\frac{Z_I e^2}{|\mathbf{r}_i-\mathbf{R}_I|} + \frac{1}{4\pi\epsilon_0}\sum_{I=1}^{K}\sum_{J>I}^{K}\frac{Z_I Z_J e^2}{|\mathbf{R}_I-\mathbf{R}_J|},\end{aligned} \tag{3.11}$$

where m_e and $\mathbf{r}_i$ are the mass and the position of electron i and M_I and $\mathbf{R}_I$ the mass and position of nucleus I. As the particles of the systems are fermions, they cannot occupy the same quantum state according to the Pauli exclusion principle,[62] meaning that the wavefunction must be antisymmetric with respect to exchange of two indistinguishable

[1] For antiparticles, the order of magnitude of the two spinors are opposite, and the energies are negative. Otherwise, the reasoning is analogous.

particles. These constraints, along with the fact that it is a many-body problem, means that the equation is intractable for anything beyond certain one-electron systems, e.g. the hydrogen atom.

3.2.1 Born-Oppenheimer approximation

A first step to reduce the problem is to assume that the electron and ion wavefunctions are separable

$$\Psi_{\text{tot}}(\mathbf{r}, \mathbf{R}) = \Psi_{\text{el}}(\mathbf{r}, \mathbf{R})\Psi_{\text{nuc}}(\mathbf{R}) \tag{3.12}$$

which is known as the Born-Oppenheimer approximation.[61, 63, 64] The approximation means that the electrons follows the movement of the nuclei instantaneously, while remaining in the same stationary state. The nuclei interacts with an average potential from the electrons and can be treated in a classical, Newtonian fashion. Intuitively, the separation is justified by the fact that the electrons are much lighter than the ions and thus that their time-scales of their dynamics are much smaller. However, this assumes that the energy associated with electron transitions are large enough to keep them in a stationary state. This does not hold for metallic systems, as the electrons have access to a continuum around the Fermi level in response to any nuclear movement. What saves us is that at temperatures much below the Fermi temperature of the metal (typically thousands of degrees), the electron transitions are limited to a small region around the Fermi level, which has little impact of most sought properties.[65]

The electron Hamiltonian may now be written as

$$\hat{H}_{\text{el}} = -\sum_{i=1}^{N} \frac{\hbar^2}{2m_e}\nabla_i^2 + \frac{1}{4\pi\epsilon_0}\sum_{i=1}^{N}\sum_{j>i}\frac{e^2}{|\mathbf{r}_i - \mathbf{r}_j|} - \frac{1}{4\pi\epsilon_0}\sum_{I=1}^{K}\sum_{i=1}^{N}\frac{Z_I e^2}{|\mathbf{r}_i - \mathbf{R}_I|}. \tag{3.13}$$

and by denoting the last term as $V_{\text{ext}}(\mathbf{r}_i)$ and using Hartree atomic units ($\hbar = m_e = e = 1/(4\pi\epsilon_0) = 1$), we have

$$\hat{H}_{\text{el}} = -\frac{1}{2}\sum_i \nabla_i^2 + \sum_i\sum_{j>i}\frac{1}{|\mathbf{r}_i - \mathbf{r}_j|} + \sum_i V_{\text{ext}}(\mathbf{r}_i). \tag{3.14}$$

The many-electron problem still remains intractable. There are essentially two ways to move forward. One way is to expand the wavefunction; the simplest way is to assume that it may be written as a linear combination of products of one-electron wave functions that satifies the antisymmetry property. This approach is called Hartree-Fock and was an early practical method for electronic structure calculations.[61, 66, 67] However, it is computationally expensive, in particular for larger systems with more than a couple of hundred electrons.

The other approach is to abandon the search for the wavefunction and instead work with the total electron density.

3.2.2 The Hohenberg-Kohn theorems

Using the electron density, $n(\mathbf{r}) = |\Psi|^2$, instead of the wavefunction to evaluate quantum mechanical properties would at least in a formal sense lower the degrees of freedom of

the system. This idea was introduced independently by Thomas and Fermi in 1927, [60, 68, 69] but the theoretical framework to justify the approach was put forward in 1964 by Hohenberg and Kohn.[70] The article is the basis for the two Hohenberg-Kohn theorems. The first of these states that the ground state electron density, $n_0(\mathbf{r})$, uniquely determines the external potential. Since the many-body Schrödinger equation in principle can be solved knowing V_{ext}, the ground state electron density uniquely defines all the solutions of the wavefunction and thus all properties of the system. The second theorem proves the existence of the universal Hohenberg-Kohn functional $F[n(\mathbf{r})]$ such that the energy functional

$$E[n(\mathbf{r})] = \int V_{\text{ext}}(\mathbf{r}) n(\mathbf{r}) \, \mathrm{d}\mathbf{r} + F[n(\mathbf{r})] \tag{3.15}$$

has its global minimum at the ground state energy, for all possible $V_{\text{ext}}(\mathbf{r})$. However, since we have only rewritten the original problem, finding $F[n(\mathbf{r})]$ would be equivalent to solving the many-body problem and is thus equally intractable.

3.2.3 The Kohn-Sham approach

In 1965, Kohn and Sham proposed a method for handling the universal functional.[65, 71] The idea is to replace the real, interacting electrons with independent particles moving in an effective potential, such that the electron densities are the same.

The Kohn-Sham electrons, with occupied orbitals ψ_i, have the electron density

$$n(\mathbf{r}) = \sum_{i=1}^{N} |\psi_i(\mathbf{r})|^2 \tag{3.16}$$

and kinetic energy[2]

$$T_0 = -\frac{\hbar^2}{2m} \sum_{i=1}^{N} \langle \psi_i | \nabla^2 | \psi_i \rangle. \tag{3.17}$$

T_0 is easy to calculate and makes up the second largest part of the energy.[72] The largest contribution comes from the interaction between the electron from the average of the other electrons, i.e. from the total electron density, the Hartree energy

$$E_{\text{H}}[n] = \frac{1}{2} \int \int \frac{n(\mathbf{r}) n(\mathbf{r}')}{|\mathbf{r} - \mathbf{r}'|} \, \mathrm{d}\mathbf{r} \, \mathrm{d}\mathbf{r}'. \tag{3.18}$$

Since the electron density includes the electron in question, this means that E_{H} inherently contains a so-called *self-interaction error*, which must be taken into account by other means.

The left-out energy contributions are exchange, which assures that the Pauli principle is upheld, and correlation containing the rest of the many-body effects, including $T - T_0$. In standard DFT, these are lumped together to the exchange-correlation energy E_{xc}. It

[2] T_0 does not correspond to the real kinetic energy, because the Kohn-Sham orbitals are different from the real ones, even if the electron densities would match.

must be approximated, which is discussed in the next section 3.3. The total energy can now be expressed as

$$E = \int V_{\text{ext}}(\mathbf{r}) n(\mathbf{r}) \, \mathrm{d}\mathbf{r} + T_0 + E_{\text{H}} + E_{\text{xc}}. \tag{3.19}$$

By application of the variational principle, we derive the Kohn-Sham equation for electron i,

$$-\frac{1}{2}\nabla^2 \psi_i(\mathbf{r}) + \left[V_{\text{ext}}(\mathbf{r}) + \int \frac{n(\mathbf{r}')}{|\mathbf{r} - \mathbf{r}'|} \, \mathrm{d}\mathbf{r}' + \frac{\delta E_{\text{xc}}}{\delta n(\mathbf{r})} \right] \psi_i(\mathbf{r}) = \varepsilon_i \psi_i(\mathbf{r}). \tag{3.20}$$

Note that the Kohn-Sham orbitals ψ_i and the Kohn-Sham energies ε_i are not the same as the real orbitals or energies, but only exist to find the true electron density, $n(\mathbf{r})$, and the energy,

$$E[n] = \sum_{i=1}^{N} \varepsilon_i - E_{\text{H}}[n] - \int n(\mathbf{r}) V_{\text{xc}}[n(\mathbf{r})] \, \mathrm{d}\mathbf{r} + E_{\text{xc}}[n]. \tag{3.21}$$

A typical DFT implementation solves the Kohn-Sham equations, with an appropriate choice of exchange-correlation functional. Starting with an initial guess of $n(\mathbf{r})$, e.g. a sum of atomic orbitals, the equations are solved iteratively until self-consistency.

3.3 Exchange-correlation functional

As seen above, the exchange-correlation functional is the hard part of DFT calculations. The exact exchange-correlation functional is not known, and, since finding it would be at least as hard as solving the classical many-body problem. We are left with using different levels of approximations, which can be ordered on the so-called Jacob's ladder from the Hartree world to the heaven of chemical accuracy.[73] Going higher on the ladder hopefully increases accuracy but definitely increases computational costs.

A natural starting point for approximations is the homogeneous electron gas, which is a decent model for metallic systems. The exchange energy, ϵ_{x}, is given exactly as[65]

$$\epsilon_{\text{x}}^{\text{h}}[n] = -\frac{3}{4}\left(\frac{3n}{\pi}\right)^{\frac{1}{3}} \tag{3.22}$$

while the correlation energy, $\epsilon_{\text{C}}^{\text{h}}$, has been computed with Monte Carlo simulations to high numerical accuracy.[74] With help of this, and assuming that the electron density behaves locally as the homogeneous electron gas, we can make approximations of the exchange-correlation functional for a general system by expansion in terms of the derivatives of the electron density.

The first approximation is the local density approximation (LDA),[71] which locally only depends on the value of $n(\mathbf{r})$. We have

$$E_{\text{xc}}^{\text{LDA}} = \int n(\mathbf{r}) \epsilon_{\text{xc}}^{\text{h}}[n(\mathbf{r}), \mathbf{r}] \, \mathrm{d}\mathbf{r}. \tag{3.23}$$

Usually, the accuracy provided by LDA is not enough. The next step is to add dependence of the gradient of $n(\mathbf{r})$, in the generalised gradient approximation (GGA)[75–78]

$$E_{\mathrm{xc}}^{\mathrm{GGA}} = \int n(\mathbf{r})\epsilon_{\mathrm{xc}}^{\mathrm{h}}[\nabla n(\mathbf{r}), n(\mathbf{r}), \mathbf{r}]\,\mathrm{d}\mathbf{r}. \tag{3.24}$$

A relatively computationally cheap and overall accurate GGA functional was introduced by John Perdew, Kieron Burke, and Matthias Ernzerhof in 1996.[79] Being one of the first exchange-correlation functionals with these good properties, the so-called PBE functional has become one of the most popular choices of exchange-correlation functional. However, PBE has a number of drawbacks in terms of accuracy for certain systems; a particular case in this project is its lack of long-range dispersion, which is discussed below. In addition to PBE, there are a number of other GGA functionals. Some of them have been developed as a response to the weak points of PBE, while others have been fitted to chemical data.

The third level on the ladder includes dependence on the second derivative of the electron density, $\nabla^2 n(r)$, which can be interpreted as the kinetic energy of the Kohn-Sham electrons. [80] This is called Meta-GGA.

On levels above LDA, it is possible to improve accuracy by including exact exchange, i.e. perfect obedience to the Pauli exclusion principle for fermions. Exact exchange is obtained from Hartree-Fock theory, which is a wavefunction based theory. In practice, hybrid functionals are constructed by calculating Hartree-Fock exchange for the Kohn-Sham orbitals, which is mixed into the rest of the DFT solution.[81] These can calculate e.g. band gaps accurately, but are very computationally expensive.[82]

3.3.1 Long range dispersion

Exchange-correlation functionals in the lowest steps of Jacob's ladder are local or semi-local in nature, and can not model long range effects.[72] In particular, London dispersion forces between instantaneous multipoles, stemming from quantum fluctuations,[3][83] are missed out.[84] There are several approaches to add dispersion to GGA functionals:

A simple model, proposed by e.g. Grimme,[85] is to parametrise the interaction by introducing pairwise terms, proportional to $1/r^6$ at medium to large distances, similar to the Lennard-Jones potential.[86] However, the approximation that the total interaction can be obtained by summing of pair potentials is inaccurate for many systems, as a third (forth, fifth etc.) atom influences the dynamic multipoles in the pair.[87]

Lundqvist et al.[88, 89] put forward the idea of calculating the total correlation as the sum of a local and a non-local contribution

$$E_{\mathrm{c}} = E_{\mathrm{c}}^{\mathrm{l}} + E_{\mathrm{c}}^{\mathrm{nl}}, \tag{3.25}$$

where $E_{\mathrm{c}}^{\mathrm{l}}$ is approximated as the LDA correlation and

$$E_{\mathrm{c}}^{\mathrm{nl}} = \frac{1}{2}\int n(\mathbf{r})\phi_k(\mathbf{r}, \mathbf{r}')n(\mathbf{r}')\,\mathrm{d}\mathbf{r}\,\mathrm{d}\mathbf{r}', \tag{3.26}$$

[3]London dispersion is some times used interchangeably with van der Waals. Strictly speaking, van der Waals includes London dispersion, as well as e.g. interactions between permanent dipoles, and permanent-induced dipole pairs.

where ϕ_k is a generating response function known as the kernel. The choice of exchange fell on a variant of PBE (revPBE)[90], and this functional is called vdW-DF.[89] By instead choosing fitted exchange proposed by Becke,[76, 91, 92] Klimeš et al. developed the optB88-vdW and optB86b-vdW.[93, 94] Another variety is to use training on chemical data sets with machine learning to get a bayesian error estimation functional (BEEF-vdW) [95].

3.3.2 Spin

In order to model magnetic and open shell systems correctly, we need to include spin. From equation 3.8 we know that the wavefunction in the non-relativistic regime is a two-component spinor coupled with the magnetic field. In the Kohn-Sham approach (equation 3.19) we see that the kinetic energy, depending on ψ_i, is trivially split into the two components, while the external and Hartree potentials only depend on the total electron density. The coupling is therefore contained in the exchange-correlation functional,

$$\epsilon_{\text{xc}} = \epsilon_{\text{xc}}[n_\uparrow, n_\downarrow], \tag{3.27}$$

which would mean that the generalisation in the case of LDA, the local spin density approximation (LSDA),[96, 97] would be

$$E_{\text{xc}}^{\text{LSDA}}[n_\uparrow, n_\downarrow] = \int \Big(n_\uparrow(\mathbf{r}) + n_\downarrow(\mathbf{r})\Big)\epsilon_{\text{xc}}^{\text{h}}[n_\uparrow(\mathbf{r}), n_\downarrow(\mathbf{r}), \mathbf{r}]\,\mathrm{d}\mathbf{r}. \tag{3.28}$$

$\epsilon_{\text{xc}}^{\text{h}}$ would in this case be a linear combination of exchange-correlation for fully polarised and unpolarised homogeneous electron gas. The spin versions of GGA and higher exchange-correlation functions are found in an analogous fashion.

3.4 Hellmann-Feynman theorem

If the Hamiltonian depends on a parameter λ, we have[98]

$$\frac{\mathrm{d}E_\lambda}{\mathrm{d}\lambda} = \langle\Psi_\lambda|\frac{\partial\hat{H}_\lambda}{\partial\lambda}|\Psi_\lambda\rangle. \tag{3.29}$$

which is known as the Hellmann-Feynmann theorem. A special case of λ of interest is the coordinate of nucleus I, $\mathbf{R}_I$. This derivative will give us the force on nucleus I. From the many-body Hamiltonian (equation 3.11), and under the Born-Oppenheimer assumption that the nuclei interact with the average of the electron cloud, we get

$$\begin{aligned} -\frac{\partial E}{\partial \mathbf{R}_I} &= \langle\Psi| - \frac{\partial\hat{H}}{\partial\mathbf{R}_I}|\Psi\rangle \\ &= \int n(\mathbf{r})\frac{Z_I(\mathbf{r}-\mathbf{R_I})}{|\mathbf{r}-\mathbf{R}_I|^3}\mathrm{d}\mathbf{r} + \sum_{J\neq I}\frac{Z_I Z_J(\mathbf{R}_I-\mathbf{R}_J)}{|\mathbf{R}_I-\mathbf{R}_J|^3} \end{aligned} \tag{3.30}$$

which is the same as the classical expression. For practical purposes, this means that both the energy and the force can be calculated in a single-point calculation.

3.4.1 Second derivative

The Hellmann-Feynman theorem can in principle be extended to the second derivative of a parameter, namely [99, 100]

$$\frac{\mathrm{d}^2 E_\lambda}{\mathrm{d}\lambda^2} = \langle \Psi_\lambda | \frac{\partial^2 \hat{H}_\lambda}{\partial \lambda^2} | \Psi_\lambda \rangle + 2 \langle \frac{\partial \Psi_\lambda}{\partial \lambda} | (E_\lambda - \hat{H}_\lambda) | \frac{\partial \Psi_\lambda}{\partial \lambda} \rangle. \tag{3.31}$$

However, it is not possible to calculate the second term in standard DFT, since the wave function and its derivatives are not directly accessible. Instead, the second derivative with respect to nuclear coordinates (the Hessian matrix) can be calculated numerically with finite differences, or analytically with more complex methods, such as the coupled-perturbed Kohn-Sham method,[101] the fragmented molecular orbital method,[102] and auxiliary density pertubation theory.[103]

3.5 Basis sets and periodicity

When solving the Kohn-Sham equations computationally, the orbitals must be expanded in a basis set χ_j

$$\psi_i = \sum_j^K c_{ij} \chi_j, \tag{3.32}$$

where the size of the basis set, K, in principle is infinite, but limited in practical application.[61] Insertion in equation 3.21,

$$\sum_j c_{ij} \hat{H} | \chi_j \rangle = \varepsilon_i \sum_j c_{ij} | \chi_j \rangle, \qquad i = 1, 2, 3, \ldots, N \tag{3.33}$$

and multiplying with the complex-conjugate $\langle \chi_k |$, we obtain

$$\sum_j c_{ij} \langle \chi_k | \hat{H} | \chi_j \rangle = \varepsilon_i \sum_j c_{ij} \langle \chi_k | \chi_j \rangle, \qquad i = 1, 2, 3, \ldots, N. \tag{3.34}$$

Introducing the shorthand notation $H_{kj} = \langle \chi_k | \hat{H} | \chi_j \rangle$, $S_{kj} = \langle \chi_k | \chi_j \rangle$ and omitting the i in the coefficients, we have

$$H_{kj} C_j = \varepsilon_i S_{kj} C_j, \qquad i = 1, 2, 3, \ldots, N, \quad k = 1, 2, 3, \ldots, K \tag{3.35}$$

which may be written on matrix form as

$$(\mathbf{H} - \varepsilon_i \mathbf{S})\, \mathbf{C} = \mathbf{0}, \qquad i = 1, 2, 3, \ldots, N. \tag{3.36}$$

This is a generalised eigenvalue problem for ε_i with the Hamiltonian matrix $\mathbf{H}$, the overlap matrix $\mathbf{S}$ and the basis coefficient vector $\mathbf{C}$.

3.5.1 Plane-waves

A natural choice of basis set for a periodic system is plane-waves.[60] Since plane-waves are orthogonal, the overlap matrix **S** reduces to the identity matrix. In the work presented here, the plane-wave based Vienna Ab-initio Simulation Package (VASP)[104, 105] was used for all calculations. The Kohn-Sham orbitals are expanded in a Fourier series

$$\psi_i = \sum_{\mathbf{k}} c_{i\mathbf{k}} e^{i\mathbf{k}\cdot\mathbf{r}}, \tag{3.37}$$

where the i in the exponent is the imaginary number. The series is truncated so that the kinetic energy of the plane-waves are smaller than a cut-off energy, i.e.

$$\frac{\hbar^2 k^2}{2m_e} < E_{\text{cut}}. \tag{3.38}$$

When a low cut-off is used, only smooth changes of the orbitals are accurately described. Including higher wave numbers will describe more rapid features and ultimately converge more or less monotonically. Rapidly changing core electronic orbitals are hard to converge, but it can be avoided by combining the plane-wave basis set with pseudopotentials, i.e. that the core electrons are not treated as electrons but lumped together with the potential from the nucleus.[106, 107] This approximation is often acceptable, since the behaviour of the valence electrons is normally what decides the properties of an atomic system.

K-point sampling and smearing

Working with a periodic system, it is natural to Fourier transform it to perform calculations in reciprocal space (k-space). Implementation of the Kohn-Sham integrals is carried out as a summation over well chosen k-points.[108] The discrete nature of the k-point sampling can lead to a convergence problem: An electron close to the Fermi level can in one iteration be placed in one orbital, which in turn changes the electron structure. The new electron structure makes it beneficial for the electron to move to a new orbital, which gives the original (or similar) electron structure. A remedy to this oscillatory behaviour is electron smearing, i.e. allowing partial occupation of orbitals.[109] One example is to let the electrons be Fermi-Dirac distributed at a fictive electron temperature greater than zero. Once the system has converged, the energy is extrapolated back to 0 K.

Chapter 4

Applied electronic structure calculations

> “
> Knowing is not enough; we must apply. Willing is not enough; we must do.
>
> – Johann Wolfgang von Goethe

Several types of electronic structure calculations, of which DFT is one, allow us to calculate the energy of a system of atoms for a certain geometry. However, single energies have no physical meaning. In order to determine physical properties, such as adsorption sites, adsorption energy, spectroscopic vibration energies and reaction free energy, we need to consider applications, such as energy optimisation, vibrational analysis, and thermodynamics.

4.1 Relaxation

Most properties we are interested in are calculated in an energetically local minimum, i.e. a configuration where any displacement results in a higher energy. To find a local minimum, we need to determine the forces along each coordinate,

$$f_i = \frac{\partial E}{\partial R_i} \tag{4.1}$$

and follow the gradient until the norm of each f_i is below a certain limit, e.g. $0.02\,\mathrm{eV/Å}$.[61] The fact that the force can be evaluated for each single point calculation simplifies the process.

4.2 Adsorption and reaction energies

In computational codes like VASP, the absolute energy of a system is highly dependent on parameters like exchange-correlation functional. Differences of energies are less sensitive, due to cancellation of errors.

In order to compute the adsorption energy of species A on top of a surface $*$, three calculations are required: One of A in gas phase (A_g), one with adsorbed A ($A*$) and one with surface only ($*$). The adsorption energy is calculated as

$$E_\mathrm{ads}(A) = E_\mathrm{tot}(A*) - E_\mathrm{tot}(*) - E_\mathrm{tot}(A_\mathrm{g}) \tag{4.2}$$

With this definition, we have that $E_\mathrm{ads} < 0$ means that adsorption is energetically favourable.

The calculation of reaction energies are made in an analogous way. Let us say that we have the following reaction

$$\mathrm{A}^* \longrightarrow \mathrm{B}^* + \mathrm{C}^* + \mathrm{D}_\mathrm{g}.$$

Then, the reaction energy would be calculated as

$$E_{\mathrm{reac}} = E_{\mathrm{tot}}(B*) + E_{\mathrm{tot}}(C*) + E_{\mathrm{tot}}(D_\mathrm{g}) - E_{\mathrm{tot}}(*). \tag{4.3}$$

4.3 Vibrational analysis

The molecules and adsorbates of interest vibrate around the energetic minimum found by a relaxation. A way to interpret this is to compare bonds to springs counteracting displacements from the equilibrium. Calculations of vibrational frequencies are useful to compare with spectroscopic measurements and to calculate thermodynamic properties.

Vibrational frequencies are calculated using the theory of small oscillations.[110] This assumes that the energy landscape is locally harmonic around the equilibrium, which means that the vibration modes can be obtained by diagonalising the mass-weighted Hessian matrix (see Appendix). Classically, these modes can have any energy, but quantum mechanics dictates that only the following energy levels are allowed:

$$E_{m,j} = \left(j + \frac{1}{2}\right)\hbar\omega_i, \qquad m = 0, 1, 2, \ldots \tag{4.4}$$

A gas-phase species will have three modes corresponding to translation and three corresponding to rotation (two for a linear molecule). These will yield near-zero frequencies (imaginary if the curvature is negative) in the vibrational analysis scheme and must be treated separately. The remaining modes are often treated as vibrations, but for practical purposes a cut-off frequency could be introduced.

4.4 Statistical mechanics

In principle, DFT calculations are carried out at 0 K while pressure remains somewhat undefined. In order to relate the obtained energies to what can be observed at realistic conditions, we need to use thermodynamics and statistical mechanics.

We consider our surface reactions to occur at the ambient temperature (293 K) and pressure (1 atm). This means that we are in the isothermic-isobaric ensemble, for which the Gibbs free energy is minimised. This is given by

$$G = U_{\mathrm{int}} + pV - TS, \tag{4.5}$$

where U_{int} is the internal energy, p pressure, V volume, T temperature and S entropy. For adsorbates, we consider the small volume changes to be negligable and approximate G with Helmholtz free energy

$$F = U_{\mathrm{int}} - TS. \tag{4.6}$$

For a gas-phase species, we assume the ideal gas approximation, where

$$V = NRT/p. \tag{4.7}$$

In both these cases, we see that we can consider the volume to be constant and make our derivations in the canonical (NVT) ensemble. For further reading on the derivations below, see Stoltze[111], Chorkendorff and Niemantsverdiet[9], and the documentation for the Atomic Simulation Environment.[112]

4.4.1 Free energy for gas phase species

We can calculate the total gas phase partition function as

$$Z = \frac{z^N}{N!} \tag{4.8}$$

where z is the partition function for a single particle and n is the number of adsorbates. The reason for the simple product is the assumption that the particles do not interact with each other, and the $n!$ factor stems from the fact that gas phase species are indistinguishable.

The single particle partition function can be written as a Boltzmann sum over all possible energies

$$z = \sum_i e^{-\beta\varepsilon_i}. \tag{4.9}$$

where $\beta = 1/k_\mathrm{B}T$. We consider a given total energy level to be separable into independent modes, m, with energy levels j_m, i.e.

$$\varepsilon_i = \varepsilon_{j_1,j_2,\ldots} = \sum_m \varepsilon_{j_m}, \tag{4.10}$$

where each mode m can occupy a separate set of energy levels.

This means that we can write z as a product, since

$$\begin{aligned} z &= \sum_i e^{-\beta\varepsilon_i} && (4.11)\\ &= \sum_{j_1,j_2,\ldots} e^{-\beta\sum_m \varepsilon_{j_m}} && (4.12)\\ &= \prod_m \Big(\sum_{j_m} e^{-\beta\varepsilon_{j_m}}\Big) && (4.13)\\ &= \prod_m z_m. && (4.14) \end{aligned}$$

We consider electronic, translational, rotational and vibrational contributions to the partition function, which are derived in Appendix:

$$z_\mathrm{el} = 2s + 1, \tag{4.15}$$

$$z_{\mathrm{tr}} = \left(\frac{2\pi m k_{\mathrm{B}} T}{h^2}\right)^{1.5} V, \tag{4.16}$$

$$z_{\mathrm{rot}} = \begin{cases} \frac{8\pi^2 I k_{\mathrm{B}} T}{\sigma h^2} & \text{for linear molecules} \\ \frac{\pi^{7/2}}{\sigma h^3}(8 k_{\mathrm{B}} T)^{3/2}\sqrt{I_A I_B I_C} & \text{for non-linear molecules} \end{cases} \tag{4.17}$$

and

$$z_{\mathrm{vib},m} = \frac{1}{1 - e^{-\beta\hbar\omega_m}}. \tag{4.18}$$

Note that the N dependence of the logarithm of the partition function is taken care of neatly since

$$\begin{aligned} \ln Z &= \ln \frac{z^N}{N!} && (4.19)\\ &= N(\ln z_{\mathrm{tr}} + \ln z_{\mathrm{el}} z_{\mathrm{rot}} z_{\mathrm{vib}}) - \ln N! && (4.20)\\ &\approx N\left(\ln V + \ln\left(\frac{2\pi m k_B T}{h^2}\right)^{1.5} + \ln z_{\mathrm{el}} z_{\mathrm{rot}} z_{\mathrm{vib}}\right) - N\ln N - N && (4.21)\\ &= N\left(\ln \frac{k_{\mathrm{B}} T}{p} - 1 + \ln\left(\frac{2\pi m k_B T}{h^2}\right)^{1.5} + \ln z_{\mathrm{el}} z_{\mathrm{rot}} z_{\mathrm{vib}}\right) && (4.22) \end{aligned}$$

which divided by N (i.e. per particle) is not dependent on the number of particles.

Since the Helmholtz free energy is the thermodynamic potential in the canonical ensemble, it is simply related to the partition function by[1]

$$\Delta F = -k_{\mathrm{B}} T \ln Z \tag{4.23}$$

where $\Delta F = F - F_0$, and F_0 is the Helmholtz free energy at 0 K. This is the same as internal energy at 0 K, i.e.

$$U_{\mathrm{int},0} = E_{\mathrm{el}} + E_{\mathrm{ZP}} \tag{4.24}$$

where E_{el} is the electronic energy from the DFT calculation and E_{ZP} the zero point vibrational energy. To this, we need to add a term of electric work,

$$W_{\mathrm{el}} = n_e e U_{\mathrm{RHE}} \tag{4.25}$$

corresponding to the energy gained or lost by moving n_e electrons, with charge e, over the electric potential U_{RHE}. As $G = F + pV$ and $pV = k_{\mathrm{B}}T$ for an ideal gas, we simply have

$$G = E_{\mathrm{el}} + E_{\mathrm{ZP}} + k_{\mathrm{B}} T(1 - \ln Z) - n_e e U_{\mathrm{ref}} \tag{4.26}$$

If the pressure is changed, this can be adjusted for by adding the term

$$\Delta G_p = k_{\mathrm{B}} T \ln \frac{p}{p_{\mathrm{ref}}} \tag{4.27}$$

where p_{ref} is the reference pressure.

[1] The thermodynamic energies are given per particle, and not the total quantity of the system.

Some other quantities

We can calculate the entropy S from F. Since

$$\mathrm{d}F = -S\,\mathrm{d}T - p\,\mathrm{d}V \tag{4.28}$$

we can derive the dependence of S on Z as

$$S = \Big(\frac{\partial F}{\partial T}\Big)_V = k_\mathrm{B}\ln Z + k_\mathrm{B}T\Big(\frac{\partial \ln Z}{\partial T}\Big)_V. \tag{4.29}$$

The internal energy can be calculated as

$$\begin{aligned}\Delta U_\mathrm{int} &= \Delta F + TS \\ &= F - T\Big(\frac{\partial F}{\partial T}\Big)_V \\ &= k_\mathrm{B}T\ln Z - T\bigg(k_\mathrm{B}\ln Z + k_\mathrm{B}T\Big(\frac{\partial \ln Z}{\partial T}\Big)_V\bigg) \\ &= k_\mathrm{B}T^2\Big(\frac{\partial \ln Z}{\partial T}\Big)_V\end{aligned} \tag{4.30}$$

Plugging in z_tr and z_rot will give $\frac{1}{2}k_\mathrm{B}T$ for each degree of freedom, which is to be expected classically.[31] This is because the partition functions have been derived in the classical limit. The electronic partition function will not contribute to the energy, which is inherently related to the assumption that only the ground state is occupied at relevant temperatures. The vibrational contribution can be computed quantum mechanically as

$$\Delta U_\mathrm{int,vib} = \sum_m \frac{\hbar\omega_m}{e^{\beta\hbar\omega_m} - 1}. \tag{4.31}$$

Thus, we have

$$U_\mathrm{int} = E_\mathrm{el} + E_\mathrm{ZP} + \frac{x}{2}k_\mathrm{B}T + \sum_m \frac{\hbar\omega_m}{e^{\beta\hbar\omega_m} - 1} - n_e e U_\mathrm{RHE} \tag{4.32}$$

where $x = 5$ for a linear molecule and $x = 6$ for a non-linear molecule. If we are interested in the enthalpy, it can be calculated as

$$H = U_\mathrm{int} + pV = U_\mathrm{int} + k_\mathrm{B}T. \tag{4.33}$$

In principle, Gibbs free energy could be calculated as

$$G = H - TS \tag{4.34}$$

but as long as there is no need for computing H or S, it is more straightforward to use Equation 4.26 directly.

4.4.2 Free energy for adsorbates

We consider adsorbates to be fixed at the surface. This means that the adsorbates are distinguishable (by their position on the infinite surface) so that the adsorbate partition function is given as

$$Z = z^N. \tag{4.35}$$

No translation nor rotation are allowed, so all degrees of freedom are vibrational. This is called the *harmonic approximation*.[113] Furthermore, even if an adsorbate would have an open shell in gas phase, we consider the its spin to be quenched by the sea of free electrons in an extended metallic surface with no net spin. Thus, we get the approximate Gibbs free energy as

$$G \approx F = E_{\mathrm{el}} + E_{\mathrm{ZP}} - k_{\mathrm{B}}T \sum_m \ln z_{\mathrm{vib},m} - n_e e U_{\mathrm{RHE}}. \tag{4.36}$$

Chapter 5

Summary of papers and outlook

> ”
> An expert is someone who has made all the mistakes which can be made in a narrow field.
>
> – Niels Bohr

5.1 Paper I

The first paper covers glycerol adsorption on Au(111), studied with DFT. We recognise that dispersion effects are important to model correctly on gold, owing to its nobility. Thus, a number of dispersion-corrected functionals were tested on a model system, methanol adsorbed on gold, to select an appropriate exchange-correlation functional. Structural, electronic, and vibrational properties were investigated on bare and surface-alloyed Au(111).

5.2 Paper II

The second paper investigates glycerol electrooxidation on gold in acidic media. The restriction to acidity stems, from a computational point of view, from limits of the validity of the theoretical model. The DFT calculations on the electrooxidation reaction are perfomed on a bare Au(111) surface, which is confirmed with the calculated surface Pourbaix diagram to be valid. However, at higher pH, the surface is reported to be at least partially covered with *OH,[114] in addition to glycerol being protolysed in the electrolyte,[115] which may alter the reaction mechanism.

We show that there is a small but detectable activity at 0.5 V vs. the reversible hydrogen electrode. This agrees with the calculated theoretical onset potential. Furthermore, we find glycerol oxidation to take place on the cathodic scan, which remains to be explained in future work.

5.3 Paper III

The third paper investigates methanol electrooxidation theoretically, focusing on dispersion and microsolvent effects. We show that the addition of dispersion effects confirms the reaction mechanism in liteature[116], while it has significant impact on the onset potential, lowering it to 0.6 V vs. RHE. This, however, does not agree with experimental reports of 1.1–1.2 V.[117]

To explain the discrepancy, we investigate a simple microsolvent model – inclusion of a single water molecule. We find that inclusion of water has some impact on the structure, but the reaction mechanism and onset potential are more or less the same as without water. This leads us to suspect that kinetics plays an important role in methanol electrooxidation on gold.

5.4 Outlook

We have gained insights in the mechanism of glycerol and methanol oxidation on gold, but there remain questions to be answered. Electrochemical kinetics of the reactions is a natural next step to take, especially in the light of the conclusion of **Paper III**. Furthermore, it would be interesting to pursue an explanation of glycerol oxidation on the cathodic scan discussed in **Paper II**, in cooperation with experimental colleagues.

Appendix

A Normal mode analysis

In order to find the normal modes of vibration, we need to solve the classical Lagrangian equations. Given a potential energy landscape, in our case calculated with DFT, the forces are computed using a central differential quotient. For further details on this derivation, see Goldstein et al.[110] and Van den Bossche.[118]

Let us expand the potential energy in the vicinity of a stable equilibrium. If x_i denote deviations for atom i, we may expand it in a Maclaurin series:

$$V(x_1, \ldots, x_n) = V(0, \ldots, 0) + \sum_i \Big(\frac{\partial V}{\partial x_i}\Big) x_i + \frac{1}{2} \sum_{i,j} \Big(\frac{\partial^2 V}{\partial x_i \partial x_j}\Big) x_i x_j + \cdots . \tag{5.1}$$

We may choose the potential in the equilibrium to be 0, and, since we have an equilibrium, all forces are zero. Assuming the deviations to be small, we are left with the quadratic terms of the expansion:

$$V = \frac{1}{2} \sum_{i,j} \Big(\frac{\partial^2 V}{\partial x_i \partial x_j}\Big) x_i x_j = \frac{1}{2} \sum_{i,j} V_{ij} x_i x_j \tag{5.2}$$

where V_{ij} is a shorthand notation for the second derivatives of the potential. These can be obtained by sampling the potential energy or the forces around the equilibrium and applying finite differences, or by more elaborate analytic methods mentioned in section 3.4.1.

On matrix form, Equation 5.2 can be written as

$$V = \frac{1}{2} \mathbf{x}^{\mathrm{T}} \mathbf{V} \mathbf{x} \tag{5.3}$$

where $\mathbf{V}$ is the Hessian matrix. By introducing mass-weighted coordinates,[1]

$$q_i = \sqrt{m_i} x_i, \tag{5.4}$$

we can rewrite the Hessian expression to

$$\frac{1}{2} \mathbf{q}^{\mathrm{T}} \mathbf{U} \mathbf{q} \tag{5.5}$$

where $U_{ij} = V_{ij}/(m_i m_j)^{1/2}$. The kinetic energy is given by

$$T = \frac{1}{2} \sum_i m_i \dot{x}_i^2 = \frac{1}{2} \dot{\mathbf{q}}^{\mathrm{T}} \dot{\mathbf{q}} \tag{5.6}$$

[1] Introducing mass-weighted coordinates is just a mathematical trick to simply the expression for kinetic energy. It is possible to do it in a way that is more physically intuitive, at the expense of brevity.

and thus the Lagrangian by

$$L = \frac{1}{2}(\mathbf{q}^{\mathrm{T}}\mathbf{U}\mathbf{q} - \dot{\mathbf{q}}^{\mathrm{T}}\dot{\mathbf{q}}) \tag{5.7}$$

The Lagrangian equations of motion then become

$$\ddot{\mathbf{q}} + \mathbf{U}\mathbf{q} = \mathbf{0}. \tag{5.8}$$

Making the oscillatory ansatz

$$q_j = a_j e^{-i\omega t} \tag{5.9}$$

where a_j are amplitudes and ω the angular frequency, we get

$$(\mathbf{U} - \omega^2\mathbf{I})\mathbf{a} = \mathbf{0} \tag{5.10}$$

which is an eigenvalue problem with matrix $\mathbf{U}$ and eigenvalues ω^2. $\mathbf{U}$ may be written in terms of eigenvectors $\mathbf{P}$ and eigenvalues $\mathbf{\Omega}$ as

$$\mathbf{U} = \mathbf{P}^{\mathrm{T}}\mathbf{\Omega}\mathbf{P}. \tag{5.11}$$

Note that since $\mathbf{U}$ is real and symmetric, $\mathbf{P}$ is orthogonal and thus $\mathbf{P}^{\mathrm{T}} = \mathbf{P}^{-1}$. The potential may be rewritten as

$$\begin{aligned} V &= \frac{1}{2}\mathbf{q}^{\mathrm{T}}(\mathbf{P}^{\mathrm{T}}\mathbf{\Omega}\mathbf{P})\mathbf{q} \\ &= \frac{1}{2}(\mathbf{P}\mathbf{q})^{\mathrm{T}}\mathbf{\Omega}(\mathbf{P}\mathbf{q}) \\ &= \frac{1}{2}\boldsymbol{\zeta}^{\mathrm{T}}\mathbf{\Omega}\boldsymbol{\zeta} \\ &= \frac{1}{2}\sum_i \omega_i^2\xi_i^2. \end{aligned} \tag{5.12}$$

where ζ_i are normal, mass-weighted coordinates. The kinetic energy can be rewritten in these coordinates to

$$\begin{aligned} T &= \frac{1}{2}\dot{\mathbf{q}}^{\mathrm{T}}\dot{\mathbf{q}} \\ &= \frac{1}{2}(\mathbf{P}^{\mathrm{T}}\dot{\boldsymbol{\zeta}})^{\mathrm{T}}(\mathbf{P}^{\mathrm{T}}\dot{\boldsymbol{\zeta}}) \\ &= \frac{1}{2}\dot{\boldsymbol{\zeta}}^{\mathrm{T}}\mathbf{P}\mathbf{P}^{\mathrm{T}}\dot{\boldsymbol{\zeta}} \\ &= \frac{1}{2}\dot{\boldsymbol{\zeta}}^{\mathrm{T}}\dot{\boldsymbol{\zeta}}. \end{aligned} \tag{5.13}$$

If the ζ_i are expressed as a linear combination of q_j (which is the practical case in ASE) can be converted to mass-independent coordinates y_i by dividing element-wise with $\sqrt{m_j}$. These would then correspond to actual normal displacements around the equilibrium.

B Ideal gas partition functions

For further details on these derivations, see Stoltze[111] and Chorkendorff and Niemantsverdiet[9].

B.1 Electron

The electronic partition function is related to the electronic energies in different orbital shells. With g_i degeneracies of the electronic energies ε_i, we have

$$z_{\text{el}} = \sum_i g_i e^{-\beta\varepsilon_i}. \tag{5.14}$$

Since the spacing between electronic levels are normally large relative to $k_{\text{B}}T\,(= 1/\beta)$, all but the first term can be neglected. If ε_0 is chosen to be 0, the partition function is simply the degeneracy at the ground state,

$$z_{\text{el}} = g_0 \tag{5.15}$$

For a paired molecule like H_2, the ground state is non-degenerate, which gives $g_0 = 1$. This is also true for CO, which has two unpaired electrons. For radicals having one unpaired electron, $g_0 = 2$. The O_2 is a triplet with two unpaired electrons, giving $g_0 = 3$. It can be seen that it is equivalent to write

$$z_{\text{el}} = 2s + 1 \tag{5.16}$$

where s is the spin.

B.2 Translation

The simplest model of the system of a monoatomic gas phase is the three-dimensional particle in a box in a quantum mechanical fashion. The energies of a particle in a one-dimensional box of length x is

$$\varepsilon_i = \frac{i^2h^2}{8mx^2} \tag{5.17}$$

The system is large enough to assume that the energy spacing close, i.e. the classical limit. This allows the Boltzmann sum to be replaced by integration according to

$$z_{\text{tr}} = \int_0^\infty \exp\Big(-\frac{u^2h^2}{8mx^2k_bT}\Big)du \tag{5.18}$$

With a change of variables, it becomes

$$\begin{aligned} z_{\text{tr}} &= \frac{2x\sqrt{2mk_bT}}{h}\int_0^\infty e^{-v^2}dv \\ &= \frac{\sqrt{\pi}}{2}\frac{2x\sqrt{2mk_BT}}{h} \\ &= \Big(\frac{2\pi mk_BT}{h^2}\Big)^{0.5}x. \end{aligned} \tag{5.19}$$

For a three-dimensional box of volume V, we have

$$z_{\mathrm{tr}} = \Big(\frac{2\pi m k_B T}{h^2}\Big)^{1.5} V. \tag{5.20}$$

B.3 Rotation

A linear molecule can be modelled as a quantum mechanical rigid rotor,[9] which gives the eigenenergies

$$\varepsilon_i = \frac{i(i+1)h^2}{8\pi^2 I} \tag{5.21}$$

where

$$I = \sum_k m_k r^2 \tag{5.22}$$

is the moment of inertia around the centre of mass.

E.g., for a diatomic molecule we have

$$I = \frac{m_1 m_2}{m_1 + m_2} d^2. \tag{5.23}$$

Taking the $2i+1$ levels of degeneracy into account, the partition function can be written as

$$\frac{1}{\sigma} \sum_i (2i+1) \exp\Big(-\frac{i(i+1)h^2}{8\pi^2 I k_B T}\Big) \tag{5.24}$$

where σ is the symmetry number. A low-symmetry molecules CO, with no rotational degeneracy, has $\sigma = 1$ while symmetric linear molecules like H_2 and CO_2 have $\sigma = 2$.

If the levels are close, which is true for all but the lightest molecules at all but low temperatures (for H_2, the critical temperature is 85 K), the sum can be approximated with the integral

$$\frac{1}{\sigma} \int_0^\infty (2u+1) \exp\Big(-\frac{u(u+1)h^2}{8\pi^2 I k_B T}\Big) du. \tag{5.25}$$

With the substitution $s = 8\pi^2 I k_B T / h^2$ we have

$$\begin{aligned}
z_{\mathrm{rot}} &= \frac{1}{\sigma} \int_0^\infty (2u+1) \exp\Big(-\frac{u(u+1)}{s}\Big) du \\
&= \frac{1}{\sigma} e^{1/(4s)} \int_0^\infty 2(u+\frac{1}{2}) \exp\Big(-\frac{(u+1/2)^2}{s}\Big) du \\
&= \frac{1}{\sigma} e^{1/(4s)} \int_{1/2}^\infty 2v \exp\Big(-\frac{v^2}{s}\Big) dv \\
&= \frac{1}{\sigma} e^{1/(4s)} \Big[-s \exp\Big(-\frac{v^2}{s}\Big)\Big]_{1/2}^\infty \\
&= \frac{s}{\sigma} \qquad (5.26) \\
& \qquad (5.27)
\end{aligned}$$

where $v = u + 1/2$. Resubstitution gives

$$z_{\text{rot}} = \frac{8\pi^2 I k_{\text{B}} T}{\sigma h^2} \tag{5.28}$$

In the general case with non-linear polyatomic molecules, the Hamiltonian can be expressed as

$$H = \frac{L_A^2}{2I_A} + \frac{L_B^2}{2I_B} + \frac{L_C^2}{2I_C} \tag{5.29}$$

where L_A, L_B and L_C are angular momenta and I_A, I_B and I_C are eigenvalues of the moments of inertia.[119] However, the quantification of the angular momenta is complex. As an intuitive sketch, consider the integral

$$\int_{-\infty}^{\infty}\int_{-\infty}^{\infty}\int_{-\infty}^{\infty} \exp\Big(-\frac{H(p,q)}{k_{\text{B}}T}\Big) = (2\pi I_A k_{\text{B}} T)^{1/2}(2\pi I_B k_{\text{B}} T)^{1/2}(2\pi I_C k_{\text{B}} T)^{1/2}. \tag{5.30}$$

In order to get the partition function, this integral must be multiplied by a constant. A factor of 2π accounts for a complete rotation while integration over all axes contributes with 4π. σ corrects overcounting while a factor of h in each dimension takes care of the conversion from momentum p to quantum wavenumber k giving

$$\begin{aligned} z_{\text{rot}} &= \frac{\sqrt{\pi}}{\sigma}\Big(\frac{8\pi I_A k_{\text{B}} T}{h^2}\Big)^{1/2}\Big(\frac{8\pi I_B k_{\text{B}} T}{h^2}\Big)^{1/2}\Big(\frac{8\pi I_C k_{\text{B}} T}{h^2}\Big)^{1/2} \\ &= \frac{\pi^{7/2}}{\sigma h^3}(8 k_{\text{B}} T)^{3/2}\sqrt{I_A I_B I_C}. \end{aligned} \tag{5.31}$$

The symmetry number for non-linear molecules is also related to rotational degeneracy; e.g., CH_3OH has $\sigma = 1$, CH_3O^* has $\sigma = 3$ and CH_4 has $\sigma = 12$.

B.4 Vibration

Vibrations can be modelled as j quantum mechanical harmonic oscillators with energies

$$\epsilon_l = \hbar\omega_l(n + 0.5) \tag{5.32}$$

giving

$$z_{\text{vib},l} = \sum e^{-\beta n \hbar \omega_l} = \frac{1}{1 - e^{-\beta\hbar\omega_l}}. \tag{5.33}$$

The zero point energy,

$$\frac{1}{2}\sum_j \hbar\omega_l, \tag{5.34}$$

is added separately to the ground state energy.

Acknowledgements

The work presented in this thesis was carried out at the Division of Chemical Physics at the Department of Physics and the Competence Centre for Catalysis (KCK), Chalmers University of Technology, Göteborg, Sweden.

This work is financially supported by the Swedish research council Formas.

The Competence Centre for Catalysis is hosted by Chalmers University of Technology and financially supported by the Swedish Energy Agency and the member companies AB Volvo, ECAPS AB, Haldor Topsøe A/S, Scania CV AB, Volvo Car Corporation AB and Wärtsilä Finland Oy.

The calculations were performed at NSC (Linköping) and Uppmax (Uppsala) via a SNIC grant.

I would also like to thank:

My main supervisor Anders Hellman, for being the best supervisor ever. Your optimism, encouragement, support, and accessibility means a lot to me.

My co-supervisor Björn Wickman for all the help in and outside the laboratory.

My co-supervisor and examiner Henrik Grönbeck for support and fruitful discussions.

My colleague Michael Busch for all the help and support, in particular in the glycerol oxidation work.

My colleague Adam Arvidsson for being a friendly, supportive, and cooperative colleague with a great sense of humour.

Other colleagues in the Theory Council at Chemical Physics: Matthias, Mikkel, Lin, Unni, Lucy, Alvaro, and Baochang.

Aadesh, Christian, Alexander, Mattias, Madeleine, and Michael (Bergmann) for good and cheerful coexistence and cooperation in the Electrochemistry lab.

Other colleagues at Chemical Physics, in particular my former office mates Stephan and Pooya, the Competence Centre for Catalysis and the Electrochemistry group at Gothenburg University.

Friends and family, for all your support.

Mikael Valter, Göteborg, August 2018

Bibliography

[1] B. Lindström and L. J. Pettersson. A Brief History of Catalysis. *CATTECH* **7**.4 (2003), 130–138. DOI: 10.1023/A:1025001809516.

[2] E. Fulhame. *An Essay on Combustion, with a View to a New Art of Dying and Painting. Wherein the Phlogistic and Antiphlogistic Hypotheses Are Proven Erroneous*. London : Printed for the author, by J. Cooper, 1794.

[3] J. Wisniak. The History of Catalysis. From the Beginning to Nobel Prizes. *Educación química* **21** (2010), 60–69.

[4] J. J. Berzelius. *Årsberättelsen om framsteg i fysik och kemi*. p. 245. Stockholm: Royal Swedish Academy of Sciences, 1835.

[5] Haber, Fritz. *Thermodynamik technischer Gasreaktionen: Sieben Vorlesungen*. R. Oldenburg, 1905.

[6] K. Honkala et al. Ammonia Synthesis from First-Principles Calculations. *Science* **307**.5709 (2005), 555–558. DOI: 10.1126/science.1106435.

[7] A. Hellman et al. "7.17 - Ammonia Synthesis: State of the Bellwether Reaction". *Comprehensive Inorganic Chemistry II (Second Edition)*. Ed. by J. Reedijk and K. Poeppelmeier. Amsterdam: Elsevier, 2013, pp. 459–474. DOI: 10.1016/B978-0-08-097774-4.00725-7.

[8] Y. Ji et al. Strategies to Enhance the Catalytic Performance of ZSM-5 Zeolite in Hydrocarbon Cracking: A Review. *Catalysts* **7**.12 (2017), 367. DOI: 10.3390/catal7120367.

[9] I. Chorkendorff and J. W. Niemantsverdriet. *Concepts of Modern Catalysis and Kinetics*. John Wiley & Sons, 2006.

[10] H. Härelind Ingelsten. *Catalysis for Lean NOx Reduction : Aspects of Catalyst Synthesis and Surface Acidity*. Doktorsavhandlingar vid Chalmers tekniska högskola: Ny serie 2250. Göteborg : Chalmers tekniska högsk., 2005, 2005.

[11] M. Vandichel, A. Moscu, and H. Grönbeck. Catalysis at the Rim: A Mechanism for Low Temperature CO Oxidation over Pt3Sn. *ACS Catalysis* **7**.11 (2017), 7431–7441. DOI: 10.1021/acscatal.7b02094.

[12] N. M. Martin et al. CO Oxidation and Site Speciation for Alloyed Palladium–Platinum Model Catalysts Studied by in Situ FTIR Spectroscopy. *The Journal of Physical Chemistry C* **121**.47 (2017), 26321–26329. DOI: 10.1021/acs.jpcc.7b07611.

[13] C. H. Hamann, A. Hamnett, and W. Vielstich. *Electrochemistry*. Weinheim : Wiley-VCH, cop. 2007, 2007.

[14] N. I. Kobozev and V. V. Monblanova. Über den Mechanismus der Elektrodiffusion des Wasserstoffes durch Palladium. *Acta Physiochimica U.R.S.S* **1** (1934), 611–650.

[15] B. P. Company. *BP statistical review of world energy*. 67th edition. British Petroleum Company, 2018.

[16] T. R. Anderson, E. Hawkins, and P. D. Jones. CO2, the Greenhouse Effect and Global Warming: From the Pioneering Work of Arrhenius and Callendar to Today's Earth System Models. *Endeavour* **40**.3 (2016), 178–187. DOI: 10.1016/j.endeavour.2016.07.002.

[17] S. Arrhenius and E. S. Holden. On The Influence of Carbonic Acid In The Air Upon The Temperature of the Earth. *Publications of the Astronomical Society of the Pacific* **9**.54 (1897), 14–24.

[18] T. M. L. Wigley and M. E. Schlesinger. Analytical Solution for the Effect of Increasing CO2 on Global Mean Temperature. *Nature* **315**.6021 (1985), 649–652. DOI: 10.1038/315649a0.

[19] G.-R. Walther et al. Ecological Responses to Recent Climate Change. *Nature* **416**.6879 (2002), 389–395. DOI: 10.1038/416389a.

[20] A. Dai. Drought under Global Warming: A Review. *Wiley Interdisciplinary Reviews: Climate Change* **2**.1 (2011), 45–65. DOI: 10.1002/wcc.81.

[21] W. D. Nordhaus. Economic Aspects of Global Warming in a Post-Copenhagen Environment. *Proceedings of the National Academy of Sciences* (2010), 201005985. DOI: 10.1073/pnas.1005985107.

[22] C. Hu et al. Catalytic Hydrogenation of CC and CO in Unsaturated Fatty Acid Methyl Esters. *Catalysis Science & Technology* **4**.8 (2014), 2427–2444. DOI: 10.1039/C4CY00267A.

[23] E. Karakaya, C. Nuur, and L. Assbring. Potential Transitions in the Iron and Steel Industry in Sweden: Towards a Hydrogen-Based Future? *Journal of Cleaner Production* **195** (2018), 651–663. DOI: 10.1016/j.jclepro.2018.05.142.

[24] X. Li and A. Faghri. Review and Advances of Direct Methanol Fuel Cells (DMFCs) Part I: Design, Fabrication, and Testing with High Concentration Methanol Solutions. *Journal of Power Sources* **226** (2013), 223–240. DOI: 10.1016/j.jpowsour.2012.10.061.

[25] S. Arrhenius. Über Die Reaktionsgeschwindigkeit Bei Der Inversion von Rohrzucker Durch Säuren. *Zeitschrift für Physikalische Chemie* **4U**.1 (1889), 226–248. DOI: 10.1515/zpch-1889-0416.

[26] S. R. Logan. The Origin and Status of the Arrhenius Equation. *Journal of Chemical Education* **59**.4 (1982), 279. DOI: 10.1021/ed059p279.

[27] M. Trautz. Das Gesetz der Reaktionsgeschwindigkeit und der Gleichgewichte in Gasen. Bestätigung der Additivität von Cv-3/2R. Neue Bestimmung der Integrationskonstanten und der Moleküldurchmesser. *Zeitschrift für anorganische und allgemeine Chemie* **96**.1 (1916), 1–28. DOI: 10.1002/zaac.19160960102.

[28] *Wikimedia Commons Figure: Catalysis Scheme*. 2018. URL: https://commons.wikimedia.org/wiki/File:CatalysisScheme.png.

[29] P. Sabatier. Hydrogénations et Déshydrogénations Par Catalyse. *Berichte der deutschen chemischen Gesellschaft* **44**.3 (1911), 1984–2001. DOI: 10.1002/cber.19110440303.

[30] M. Argyle et al. Heterogeneous Catalyst Deactivation and Regeneration: A Review. *Catalysts* **5**.1 (2015), 145–269. DOI: 10.3390/catal5010145.

[31] D. V. Schroeder. *An Introduction to Thermal Physics*. International Edition. San Francisco: Addison Wesley Longman, 2000.

[32] W. Nernst. Die elektromotorische Wirksamkeit der Jonen. *Zeitschrift für physikalische Chemie* **4**.1 (1889), 129–181.

[33] O. Teschke, G. Ceotto b, and E. de Souza. Interfacial Aqueous Solutions Dielectric Constant Measurements Using Atomic Force Microscopy. *Chemical Physics Letters* **326**.3-4 (2000), 328–334. DOI: 10.1016/S0009-2614(00)00780-6.

[34] *Wikimedia Commons Figure: Double Layer*. 2018. URL: https://commons.wikimedia.org/wiki/File:EDLC-Potentialdistribution.png.

[35] P. Spitzer et al. "Reference Electrodes for Aqueous Solutions". *Handbook of Reference Electrodes*. Springer, Berlin, Heidelberg, 2013, pp. 77–143. DOI: 10.1007/978-3-642-36188-3_5.

[36] Y. Cai and A. B. Anderson. The Reversible Hydrogen Electrode: Potential-Dependent Activation Energies over Platinum from Quantum Theory. *The Journal of Physical Chemistry B* **108**.28 (2004), 9829–9833. DOI: 10.1021/jp037126d.

[37] B. Wickman. "Nanostructured model electrodes for studies of fuel cell reactions". PhD thesis. 2010.

[38] M. T. M. Koper. Analysis of Electrocatalytic Reaction Schemes: Distinction between Rate-Determining and Potential-Determining Steps. *Journal of Solid State Electrochemistry* **17**.2 (2013), 339–344. DOI: 10.1007/s10008-012-1918-x.

[39] X. Shi et al. Understanding Activity Trends in Electrochemical Water Oxidation to Form Hydrogen Peroxide. *Nature Communications* **8**.1 (2017), 701. DOI: 10.1038/s41467-017-00585-6.

[40] B. Iandolo et al. The Rise of Hematite: Origin and Strategies to Reduce the High Onset Potential for the Oxygen Evolution Reaction. *Journal of Materials Chemistry A* **3**.33 (2015), 16896–16912. DOI: 10.1039/C5TA03362D.

[41] *Performing Cyclic Voltammetry Measurements Using Model 2450-EC or 2460-EC Electrochemistry Lab System*. SJ Electronics. 2016.

[42] J. Perez, E. R. Gonzalez, and H. M. Villullas. Hydrogen Evolution Reaction on Gold Single-Crystal Electrodes in Acid Solutions. *The Journal of Physical Chemistry B* **102**.52 (1998), 10931–10935. DOI: 10.1021/jp9831987.

[43] O. Diaz-Morales et al. Electrochemical Water Splitting by Gold: Evidence for an Oxide Decomposition Mechanism. *Chemical Science* **4**.6 (2013), 2334–2343. DOI: 10.1039/C3SC50301A.

[44] M. F. Vitha. *Chromatography: Principles and instrumentation*. Vol. 185. John Wiley & Sons, 2016.

[45] E. Rouya et al. Electrochemical Characterization of the Surface Area of Nanoporous Gold Films. *Journal of The Electrochemical Society* **159**.4 (2012), K97–K102. DOI: 10.1149/2.097204jes.

[46] O. Björneholm et al. Water at Interfaces. *Chemical Reviews* **116**.13 (2016), 7698–7726. DOI: 10.1021/acs.chemrev.6b00045.

[47] M. T. M. Koper. Theory of Multiple Proton–Electron Transfer Reactions and Its Implications for Electrocatalysis. *Chemical Science* **4**.7 (2013), 2710–2723. DOI: 10.1039/C3SC50205H.

[48] M. Leslie and N. J. Gillan. The Energy and Elastic Dipole Tensor of Defects in Ionic Crystals Calculated by the Supercell Method. *Journal of Physics C: Solid State Physics* **18**.5 (1985), 973. DOI: 10.1088/0022-3719/18/5/005.

[49] J. K. Nørskov et al. Origin of the Overpotential for Oxygen Reduction at a Fuel-Cell Cathode. *The Journal of Physical Chemistry B* **108**.46 (2004), 17886–17892. DOI: 10.1021/jp047349j.

[50] A. Rendón-Calle, S. Builes, and F. Calle-Vallejo. A Brief Review of the Computational Modeling of CO2 Electroreduction on Cu Electrodes. *Current Opinion in Electrochemistry* (2018). DOI: 10.1016/j.coelec.2018.03.012.

[51] E. Skúlason et al. Density Functional Theory Calculations for the Hydrogen Evolution Reaction in an Electrochemical Double Layer on the Pt(111) Electrode. *Physical Chemistry Chemical Physics* **9**.25 (2007), 3241–3250. DOI: 10.1039/B700099E.

[52] E. Skúlason et al. Modeling the Electrochemical Hydrogen Oxidation and Evolution Reactions on the Basis of Density Functional Theory Calculations. *The Journal of Physical Chemistry C* **114**.42 (2010), 18182–18197. DOI: 10.1021/jp1048887.

[53] C. D. Taylor et al. First Principles Reaction Modeling of the Electrochemical Interface: Consideration and Calculation of a Tunable Surface Potential from Atomic and Electronic Structure. *Physical Review B* **73**.16 (2006), 165402. DOI: 10.1103/PhysRevB.73.165402.

[54] G. Kastlunger, P. Lindgren, and A. A. Peterson. Controlled-Potential Simulation of Elementary Electrochemical Reactions: Proton Discharge on Metal Surfaces. *The Journal of Physical Chemistry C* **122**.24 (2018), 12771–12781. DOI: 10.1021/acs.jpcc.8b02465.

[55] K. Chan and J. K. Nørskov. Electrochemical Barriers Made Simple. *The Journal of Physical Chemistry Letters* **6**.14 (2015), 2663–2668. DOI: 10.1021/acs.jpclett.5b01043.

[56] H. A. Hansen, J. Rossmeisl, and J. K. Nørskov. Surface Pourbaix Diagrams and Oxygen Reduction Activity of Pt, Ag and Ni(111) Surfaces Studied by DFT. *Physical Chemistry Chemical Physics* **10**.25 (2008), 3722–3730. DOI: 10.1039/B803956A.

[57] P. A. M. Dirac. Quantum Mechanics of Many-Electron Systems. *Proc. R. Soc. Lond. A* **123**.792 (1929), 714–733. DOI: 10.1098/rspa.1929.0094.

[58] P. Strange. *Relativistic Quantum Mechanics : With Applications in Condensed Matter and Atomic Physics*. Cambridge : Cambridge Univ. Press, 1998, 1998.

[59] P. A. M. Dirac. The Quantum Theory of the Electron. *Proc. R. Soc. Lond. A* **117**.778 (1928), 610–624. DOI: 10.1098/rspa.1928.0023.

[60] R. M. Martin. *Electronic Structure: Basic Theory and Practical Methods*. Cambridge: Cambridge Univ. Press, 2004.

[61] J. Thijssen. *Computational Physics*. Cambridge University Press, 2007.

[62] W. Pauli. Über den Zusammenhang des Abschlusses der Elektronengruppen im Atom mit der Komplexstruktur der Spektren. *Zeitschrift für Physik* **31**.1 (1925), 765–783. DOI: 10.1007/BF02980631.

[63] M. Born and R. Oppenheimer. Zur Quantentheorie Der Molekeln. *Annalen der Physik* **389**.20 (1927), 457–484. DOI: 10.1002/andp.19273892002.

[64] B. I. Lundqvist, A. Hellman, and I. Zorić. Electron Transfer and Nonadiabaticity. *Handbook of Surface Science* **3** (2008), 429–524.

[65] J. Kohanoff. *Electronic Structure Calculations for Solids and Molecules: Theory and Computational Methods*. Cambridge: Cambridge Univ. Press, 2006.

[66] D. R. Hartree. The Wave Mechanics of an Atom with a Non-Coulomb Central Field. Part I. Theory and Methods. *Mathematical Proceedings of the Cambridge Philosophical Society* **24**.1 (1928), 89–110. DOI: 10.1017/S0305004100011919.

[67] V. Fock. Näherungsmethode zur Lösung des quantenmechanischen Mehrkörperproblems. *Zeitschrift für Physik* **61**.1 (1930), 126–148. DOI: 10.1007/BF01340294.

[68] L. H. Thomas. The Calculation of Atomic Fields. *Mathematical Proceedings of the Cambridge Philosophical Society* **23**.5 (1927), 542–548. DOI: 10.1017/S0305004100011683.

[69] E. Fermi. Un metodo statistico per la determinazione di alcune priorieta dell'atome. *Rend. Accad. Naz. Lincei* **6**.602-607 (1927), 32.

[70] P. Hohenberg and W. Kohn. Inhomogeneous Electron Gas. *Physical Review* **136**.3B (1964), B864–B871. DOI: 10.1103/PhysRev.136.B864.

[71] W. Kohn and L. J. Sham. Self-Consistent Equations Including Exchange and Correlation Effects. *Physical Review* **140**.4A (1965), A1133–A1138. DOI: 10.1103/PhysRev.140.A1133.

[72] R. O. Jones and O. Gunnarsson. The Density Functional Formalism, Its Applications and Prospects. *Reviews of Modern Physics* **61**.3 (1989), 689–746. DOI: 10.1103/RevModPhys.61.689.

[73] J. P. Perdew et al. Prescription for the Design and Selection of Density Functional Approximations: More Constraint Satisfaction with Fewer Fits. *The Journal of Chemical Physics* **123**.6 (2005), 062201. DOI: 10.1063/1.1904565.

[74] D. M. Ceperley and B. J. Alder. Ground State of the Electron Gas by a Stochastic Method. *Physical Review Letters* **45**.7 (1980), 566–569. DOI: 10.1103/PhysRevLett.45.566.

[75] D. C. Langreth and M. J. Mehl. Beyond the Local-Density Approximation in Calculations of Ground-State Electronic Properties. *Physical Review B* **28**.4 (1983), 1809–1834. DOI: 10.1103/PhysRevB.28.1809.

[76] A. D. Becke. Density-Functional Exchange-Energy Approximation with Correct Asymptotic Behavior. *Physical Review A* **38**.6 (1988), 3098–3100. DOI: 10.1103/PhysRevA.38.3098.

[77] J. P. Perdew et al. Atoms, Molecules, Solids, and Surfaces: Applications of the Generalized Gradient Approximation for Exchange and Correlation. *Physical Review B* **46**.11 (1992), 6671–6687. DOI: 10.1103/PhysRevB.46.6671.

[78] J. P. Perdew et al. Erratum: Atoms, Molecules, Solids, and Surfaces: Applications of the Generalized Gradient Approximation for Exchange and Correlation. *Physical Review B* **48**.7 (1993), 4978–4978. DOI: 10.1103/PhysRevB.48.4978.2.

[79] J. P. Perdew, K. Burke, and M. Ernzerhof. Generalized Gradient Approximation Made Simple. *Physical Review Letters* **77**.18 (1996), 3865–3868. DOI: 10.1103/PhysRevLett.77.3865.

[80] J. P. Perdew et al. Accurate Density Functional with Correct Formal Properties: A Step Beyond the Generalized Gradient Approximation. *Physical Review Letters* **82**.12 (1999), 2544–2547. DOI: 10.1103/PhysRevLett.82.2544.

[81] A. D. Becke. A New Mixing of Hartree–Fock and Local Density-functional Theories. *The Journal of Chemical Physics* **98**.2 (1993), 1372–1377. DOI: 10.1063/1.464304.

[82] A. J. Garza and G. E. Scuseria. Predicting Band Gaps with Hybrid Density Functionals. *The Journal of Physical Chemistry Letters* **7**.20 (2016), 4165–4170. DOI: 10.1021/acs.jpclett.6b01807.

[83] F. London. The General Theory of Molecular Forces. *Transactions of the Faraday Society* **33**.0 (1937), 8b–26. DOI: 10.1039/TF937330008B.

[84] E. Hult et al. Density Functional for van Der Waals Forces at Surfaces. *Physical Review Letters* **77**.10 (1996), 2029–2032. DOI: 10.1103/PhysRevLett.77.2029.

[85] S. Grimme. Semiempirical GGA-type density functional constructed with a long-range dispersion correction. *Journal of Computational Chemistry* **27**.15 (2006), 1787–1799. DOI: 10.1002/jcc.20495.

[86] J. E. Jones. On the Determination of Molecular Fields. —II. From the Equation of State of a Gas. *Proc. R. Soc. Lond. A* **106**.738 (1924), 463–477. DOI: 10.1098/rspa.1924.0082.

[87] J. F. Dobson. Beyond Pairwise Additivity in London Dispersion Interactions. *International Journal of Quantum Chemistry* **114**.18 (2014), 1157–1161. DOI: 10.1002/qua.24635.

[88] M. Dion et al. Van Der Waals Density Functional for General Geometries. *Physical Review Letters* **92**.24 (2004), 246401. DOI: 10.1103/PhysRevLett.92.246401.

[89] D. C. Langreth et al. Van der Waals density functional theory with applications. *International Journal of Quantum Chemistry* **101**.5 (2005), 599–610. DOI: 10.1002/qua.20315.

[90] Y. Zhang and W. Yang. Comment on "Generalized Gradient Approximation Made Simple". *Physical Review Letters* **80**.4 (1998), 890–890. DOI: 10.1103/PhysRevLett.80.890.

[91] A. D. Becke. Density Functional Calculations of Molecular Bond Energies. *The Journal of Chemical Physics* **84**.8 (1986), 4524–4529. DOI: 10.1063/1.450025.

[92] A. D. Becke. On the Large-gradient Behavior of the Density Functional Exchange Energy. *The Journal of Chemical Physics* **85**.12 (1986), 7184–7187. DOI: 10.1063/1.451353. (Visited on 04/19/2017).

[93] J. Klimeš, D. R. Bowler, and A. Michaelides. Chemical Accuracy for the van Der Waals Density Functional. *Journal of Physics: Condensed Matter* **22**.2 (2010), 022201. DOI: 10.1088/0953-8984/22/2/022201.

[94] J. Klimeš, D. R. Bowler, and A. Michaelides. Van Der Waals Density Functionals Applied to Solids. *Physical Review B* **83**.19 (2011), 195131. DOI: 10.1103/PhysRevB.83.195131.

[95] J. Wellendorff et al. Density Functionals for Surface Science: Exchange-Correlation Model Development with Bayesian Error Estimation. *Physical Review B* **85**.23 (2012), 235149. DOI: 10.1103/PhysRevB.85.235149.

[96] O. Gunnarsson, B. I. Lundqvist, and S. Lundqvist. Screening in a Spin-Polarized Electron Liquid. *Solid State Communications* **11**.1 (1972), 149–153. DOI: 10.1016/0038-1098(72)91150-7.

[97] O. Gunnarsson and B. I. Lundqvist. Exchange and Correlation in Atoms, Molecules, and Solids by the Spin-Density-Functional Formalism. *Physical Review B* **13**.10 (1976), 4274–4298. DOI: 10.1103/PhysRevB.13.4274.

[98] J. P. Perdew and S. Kurth. "Density Functionals for Non-Relativistic Coulomb Systems". *Density Functionals: Theory and Applications*. Lecture Notes in Physics. Springer, Berlin, Heidelberg, 1998, pp. 8–59. DOI: 10.1007/BFb0106732.

[99] B. M. Deb. Note on an Upper Bound Property of Second Derivatives of the Energy. *Chemical Physics Letters* **17**.1 (1972), 78–79. DOI: 10.1016/0009-2614(72)80329-4.

[100] M. E. H. Ismail and M. E. Muldoon. On the Variation with Respect to a Parameter of Zeros of Bessel and Q-Bessel Functions. *Journal of Mathematical Analysis and Applications* **135**.1 (1988), 187–207. DOI: 10.1016/0022-247X(88)90148-5.

[101] H. Jacobsen et al. Analytic Second Derivatives of Molecular Energies: A Density Functional Implementation. *Computer Physics Communications* **100**.3 (1997), 263–276. DOI: 10.1016/S0010-4655(96)00119-1.

[102] H. Nakata et al. Analytic Second Derivative of the Energy for Density Functional Theory Based on the Three-Body Fragment Molecular Orbital Method. *The Journal of Chemical Physics* **142**.12 (2015), 124101. DOI: 10.1063/1.4915068.

[103] R. I. Delgado-Venegas et al. Analytic Second Derivatives from Auxiliary Density Perturbation Theory. *The Journal of Chemical Physics* **145**.22 (2016), 224103. DOI: 10.1063/1.4971292.

[104] G. Kresse and J. Furthmüller. Efficiency of Ab-Initio Total Energy Calculations for Metals and Semiconductors Using a Plane-Wave Basis Set. *Computational Materials Science* **6**.1 (1996), 15–50. DOI: 10.1016/0927-0256(96)00008-0.

[105] G. Kresse and J. Furthmüller. Efficient Iterative Schemes for Ab Initio Total-Energy Calculations Using a Plane-Wave Basis Set. *Physical Review B* **54**.16 (1996), 11169–11186. DOI: 10.1103/PhysRevB.54.11169.

[106] H. Hellmann. *Hans Hellmann: Einführung in Die Quantenchemie: Mit Biografischen Notizen von Hans Hellmann Jr.* Springer-Verlag, 2015.

[107] P. Schwerdtfeger. The Pseudopotential Approximation in Electronic Structure Theory. *ChemPhysChem* **12**.17 (2011), 3143–3155. DOI: 10.1002/cphc.201100387.

[108] H. J. Monkhorst and J. D. Pack. Special Points for Brillouin-Zone Integrations. *Physical Review B* **13**.12 (1976), 5188–5192. DOI: 10.1103/PhysRevB.13.5188.

[109] M. Michelini, R. Pis Diez, and A. Jubert. A density functional study of small nickel clusters. *International journal of quantum chemistry* **70**.4-5 (1998), 693–701.

[110] C. P. P. J. L. Safko, H. Goldstein, and C. Poole. *Classical mechanics*. Pearson Education, Inc, 2002.

[111] P. Stoltze. Surface Science as the Basis for the Understanding of the Catalytic Synthesis of Ammonia. *Physica Scripta* **36**.5 (1987), 824. DOI: 10.1088/0031-8949/36/5/010.

[112] *Atomic Simulation Environment*. 2018. URL: https://wiki.fysik.dtu.dk/ase/ase/thermochemistry/thermochemistry.html.

[113] M. Jørgensen and H. Grönbeck. Adsorbate Entropies with Complete Potential Energy Sampling in Microkinetic Modeling. *The Journal of Physical Chemistry C* **121**.13 (2017), 7199–7207. DOI: 10.1021/acs.jpcc.6b11487.

[114] Y. Kwon, K. J. P. Schouten, and M. T. M. Koper. Mechanism of the Catalytic Oxidation of Glycerol on Polycrystalline Gold and Platinum Electrodes. *ChemCatChem* **3**.7 (2011), 1176–1185. DOI: 10.1002/cctc.201100023.

[115] Y. Kwon et al. Electrocatalytic Oxidation of Alcohols on Gold in Alkaline Media: Base or Gold Catalysis? *Journal of the American Chemical Society* **133**.18 (2011), 6914–6917. DOI: 10.1021/ja200976j.

[116] P. Ferrin et al. Reactivity Descriptors for Direct Methanol Fuel Cell Anode Catalysts. *Surface Science* **602**.21 (2008), 3424–3431. DOI: 10.1016/j.susc.2008.08.011.

[117] Z. Borkowska, A. Tymosiak-Zielinska, and G. Shul. Electrooxidation of Methanol on Polycrystalline and Single Crystal Gold Electrodes. *Electrochimica Acta*. Trends in Surface Electrochemistry:From Single Crystals to Nanoparticles **49**.8 (2004), 1209–1220. DOI: 10.1016/j.electacta.2003.09.046.

[118] M. Van den Bossche. "Methane Oxidation over Palladium Oxide: From Electronic Structure to Catalytic Conversion". Licentiate Thesis. 2015.

[119] *Chemistry Libre Texts*. 2018. URL: https://bit.ly/2oqtPMK.